Heavy neutral bosons and dark matter in the 3-3-1 model with axionlike particle

T. T. Hieu[1,2†] V. H. Binh[3,4‡] H. N. Long[5,6§] H. T. Hung[1,4¶]

[1]Department of Physics, Hanoi Pedagogical University 2, Phu Tho 290000, Vietnam
[2]Graduate Univesity of Sience and Technology, Vietnam Academy of Sience and Technology, Hanoi 100000, Vietnam
[3]Institute of Physics, VAST, Hanoi 100000, Vietnam
[4]Bogoliubov Laboratory of Theoretical Physics, Joint Institute for Nuclear Research, Dubna 141980, Russian Federation
[5]Subatomic Physics Research Group, Science and Technology Advanced Institute, Van Lang University, Ho Chi Minh 700000, Vietnam
[6]Faculty of Applied Technology, School of Technology, Van Lang University, Ho Chi Minh 700000, Vietnam

Abstract: We consider heavy neutral bosons in the 3-3-1 model with axionlike particles (331ALP), including the Higgs boson and the Z' boson, which lie beyond the Standard Model (SM). Based on gluon-gluon fusion at the LHC, we investigate cross-section signals in the parameter-space region consistent with current experimental limits on lepton-flavor-violating decays, including processes involving charged leptons and the Higgs boson, and we provide predictions of $m_{h_2} \geq 630$ GeV. A new gauge boson, denoted by Z', is constrained to have a mass above 5.1 TeV by analyzing the cross sections of Z'-mediated processes in combination with experimental limits from searches for high-mass dilepton resonances at ATLAS and CMS. We also consider the stability of odd-Z_2 particles, with Z_2 assumed to be a residual symmetry after spontaneous symmetry-breaking stages, to identify dark matter candidates in the model. By investigating the dark matter relic density within experimentally allowed limits, we establish a relationship between the dark matter mass and the axion-breaking scale.

Keywords: lepton-flavor-violating decays, CP-even Higgs bosons, gluon-gluon fusion at LHC, heavy neutral bosons, dark matter

DOI: 10.1088/1674-1137/aea10c **CSTR:** 32044.14.ChinesePhysicsC.51013112

I. INTRODUCTION

The hypothesis of lepton flavor violating (LFV) processes has been increasingly considered in explanations of new physics, such as the polarization of τ and the mixing of charged leptons in the two last generations in $\tau \to 3\mu$ decay at Belle-II [1], polarization probes of τ and Hyperon in quasi-elastic scattering processes [2], and the influence of LFV interactions mediated by heavy scalars with lepton number 2 (bilepton scalars) on supernova dynamics [3], among others. The neutral lepton sector is well established by the confirmed masses and oscillations of neutrinos [4, 5], and the charged lepton sector is also constrained by the following branching-ratio limits [6−10]:

$$\begin{aligned} &\mathrm{Br}(\mu \to e\gamma) \leq 4.2\times10^{-13}, \mathrm{Br}(\tau \to e\gamma) \leq 3.3\times10^{-8}, \\ &(\tau \to \mu\gamma) \leq 4.4\times10^{-8}, \end{aligned} \tag{1}$$

and the lepton-flavor-violating decays of the SM-like Higgs boson (LFVHD) also have experimental limits, as given in [11−13]

$$\begin{aligned} &\mathrm{Br}(h \to \mu\tau) \leq 10^{-3}, \mathrm{Br}(h \to \tau e) \leq 10^{-3}, \\ &\mathrm{Br}(h \to \mu e) \leq 6.1\times10^{-5}. \end{aligned} \tag{2}$$

The LFV processes are of greater interest in models beyond the Standard Model (BSM), which contain abundant sources of lepton flavor violation. They may appear alongside neutrino mass-generation mechanisms, including two main types: effective operators [14−18] and seesaw mechanisms [19−27]. Both types have yielded good results regarding LFVHD, even showing that $\mathrm{Br}(h \to \mu\tau)$ can reach $O(10^{-4})$ [28−31]. Theoretical studies have shown that LFVHD signals are much smaller

Received 8 April 2026; Accepted 1 September 2026; Accepted manuscript online 2 September 2026

† E-mail: trantrunghieu@hpu2.edu.vn
‡ E-mail: vhbinh@iop.vast.vn
§ E-mail: hoangngoclong@vlu.edu.vn
¶ E-mail: hathanhhung@hpu2.edu.vn

Content from this work may be used under the terms of the Creative Commons Attribution 3.0 licence. Any further distribution of this work must maintain attribution to the author(s) and the title of the work, journal citation and DOI. Article funded by SCOAP[3] and published under licence by Chinese Physical Society and the Institute of High Energy Physics of the Chinese Academy of Sciences and the Institute of Modern Physics of the Chinese Academy of Sciences and IOP Publishing Ltd

than the experimental limit at the LHC [32], even with contributions from Majorana neutrinos [33]. One study also pointed out that the LFVHD signal at one-loop order in BSM models is always smaller than 10^{-4} because it is suppressed by a loop factor and by constraints from charged lepton flavor violation (cLFV) [34]. Furthermore, some studies have identified a parameter-space region that satisfies the experimental limits on both cLFV and LFVHD, which is well suited for investigating other phenomena, for example, predicting the signal $(g-2)_\mu$ in the parameter-space region satisfying the experimental limits of LFVHD [35], and finding the signal of $\mathrm{Br}(Z \to e_a e_b)$ and comparing it with $\mathrm{Br}(h \to e_a e_b)$ [36]. Moreover, to explain neutral-meson oscillations and rare meson decays, tree-level quark FCNCs are often introduced through a new neutral gauge boson Z' and a singlet scalar. To accomplish this, a $U(1)_N$ symmetry is added to the SM gauge group. An interesting consequence of this model is that it naturally explains the discrepancy in the measurement of the W boson mass reported by CDF or CMS [37].

Recently, LHC experiments based on gluon-gluon fusion at a center-of-mass energy $\sqrt{s} = 13$ TeV have yielded very noteworthy results. CMS searched for a heavy neutral Higgs boson in the mass range of $200 \to 900$ GeV in the $\mu\tau$ decay mode, using a data set with an integrated luminosity of 35.9 fb^{-1}. The search set upper limits on the production cross section multiplied by the branching ratio in the range from 51.9(57.4) fb to 1.6(2.1) fb at 95% CL [38]. Furthermore, searches for high-mass resonances in the range of $250 \to 6000$ GeV have also been carried out by ATLAS (139 fb^{-1}) and CMS (140 fb^{-1}), and an important consequence is the relationship between the upper limit of the cross section times branching ratio at 95% CL and the resonant mass of the heavy neutral boson [7, 39]. Based on this relationship, one can obtain mass limits for heavy neutral bosons. This provides a promising theoretical approach for predicting the masses of heavy neutral bosons by investigating the product of the cross section and the branching ratio in a specific model.

The 3-3-1 models can provide axions that are not only naturally light but also avoid quantum-gravity effects by introducing a local Z_N ($N = 11, 13$) symmetry [40–42]. The action of Z_N, together with gauge invariance, particle content, renormalizability, and Lorentz invariance, automatically implements the Peccei-Quinn (PQ) symmetry in the classical Lagrangian. The light axion mass is resolved by adding a gauge singlet whose VEV is at the axion symmetry-breaking scale of about 10^{10} GeV in a 3-3-1 model with the gauge group $SU(3)_C \otimes SU(3)_L \otimes U(1)_X \otimes Z_{11} \otimes Z_2$ [43]. A model established on the basis of the gauge group and particle content of Ref. [43], differing only in the action of Z_2 on the fields, has provided a fairly complete Higgs-sector phenomenology [44]; it is called 331ALP for short. The 331ALP possesses many interesting properties, such as the following: the physical states of the axion-like particle and other scalar particles were obtained, the scalar-sector masses were shown to lie in the range of 100 GeV – 1 TeV based on numerical analysis, and rare top-quark decays, meson oscillations, and the lepton-flavor-conserving decay of the SM-like Higgs boson were also analyzed. However, LFV processes, the masses of heavy neutral bosons, and dark matter have yet to be considered in 331ALP. In this work, we address these issues.

The paper is organized as follows. In the next section, we review the model and give the mass spectrum of the gauge and Higgs bosons. We calculate the Feynman rules and analytic formulas for cLFV and LFVHDs in Sec. III. The Z' boson and dark matter are discussed in Sec. IV and Sec. V. Conclusions are presented in Sec. VI. Finally, we provide Appendix A, B to calculate the amplitude and show numerical results for $h_{1,2} \to \mu\tau$ decays.

II. REVIEW OF THE MODEL

A. Particle content and discrete symmetries

The fermion sector of the model and its $SU(3)_C \otimes SU(3)_L \otimes U(1)_X$ assignments are:

$$\begin{aligned}
&\psi_{aL} = (\nu_a, l_a, (\nu_{aR})^c)_L^T \sim (1,3,-1/3), l_{aR} \sim (1,1,-1), N_{aR} \sim (1,1,0),\\
&Q_{3L} = (u_3, d_3, U_3)_L^T \sim (3,3,1/3), Q_{nL} = (d_n, -u_n, D_n)_L^T \sim (3,3^*,0),\\
&u_{aR} \sim (3,1,2/3), U_{3R} \sim (3,1,2/3), d_{aR} \sim (3,1,-1/3), D_{nR} \sim (3,1,-1/3),
\end{aligned} \tag{3}$$

where $n = 1,2$ and $a = \{n,3\}$ are family indices. The $U_{3L,R}$ and $D_{nL,R}$ are exotic quarks with charges of 2/3 and –1/3, respectively, the same as the usual u-type and d-type, whereas N_{aR} and ν_{aR} are right-handed Majorana and Dirac neutrinos, respectively.

We need three $SU(3)_L$ triplet scalars, η,ρ,χ to generate mass for gauge bosons and fermions as usual in 3-3-1 models with right-handed neutrinos [15, 45]. However, in this case, we require an additional neutral $SU(3)_L$ singlet scalar, ϕ, to generate mass for exotic neutrinos. Therefore, the multiplet scalars and their vacuum expectation values (VEVs) are given as follows [43, 44, 46]:

$$\begin{aligned}
&\eta = \begin{pmatrix} \eta_1^0 \\ \eta_2^- \\ \eta_3^0 \end{pmatrix} \sim \left(1,3,-\frac{1}{3}\right), \chi = \begin{pmatrix} \chi_1^0 \\ \chi_2^- \\ \chi_3^0 \end{pmatrix} \sim \left(1,3,-\frac{1}{3}\right),\\
&\rho = \begin{pmatrix} \rho_1^+ \\ \rho_2^0 \\ \rho_3^+ \end{pmatrix} \sim \left(1,3,\frac{2}{3}\right), \phi \sim (1,1,0),
\end{aligned} \tag{4}$$

and

$$\langle\eta\rangle=\begin{pmatrix}\frac{v_\eta}{\sqrt{2}}\\0\\0\end{pmatrix},\langle\chi\rangle=\begin{pmatrix}0\\0\\\frac{v_\chi}{\sqrt{2}}\end{pmatrix},\langle\rho\rangle=\begin{pmatrix}0\\\frac{v_\rho}{\sqrt{2}}\\0\end{pmatrix},$$
$$\langle\phi\rangle=\frac{v_\phi}{\sqrt{2}}. \tag{5}$$

As shown in Eq. (4), η and χ have the same quantum numbers under the $SU(3)_C\otimes SU(3)_L\otimes U(1)_X$ group. Therefore, in the scalar self-interaction terms, non-Hermitian terms of second order, such as $\eta^\dagger\chi$, or third order, such as $\eta^\dagger\chi\phi$, necessarily appear. These terms cause many difficulties in determining the physical Higgs states. Therefore, this difficulty can be eliminated by introducing Z_{11} into the gauge group [40]. There are several different ways to assign Z_{11} charges to eliminate non-Hermitian terms, but in this work we adopt the same choice as in Ref. [44]. Then, the fields transform under Z_{11} as follows:

$$\begin{aligned}Q_{3L}&\to\omega_0 Q_{3L},\\ \psi_{aL}&\to\omega_1^1\psi_{aL},\phi\to\omega_1^{-1}\phi,\\ d_{aR}&\to\omega_2^1 d_{aR},\rho\to\omega_2^{-1}\rho,\\ (l_{aR},\,U_{3R})&\to\omega_3^1(l_{aR},\,U_{3R}),\chi\to\omega_3^{-1}\chi,\\ D_{nR}&\to\omega_4^1 D_{nR},Q_{nL}\to\omega_4^{-1}Q_{nL},\\ u_{aR}&\to\omega_5^1 u_{aR},\eta\to\omega_5^{-1}\eta,\end{aligned} \tag{6}$$

where $\omega_m\equiv e^{\frac{i2\pi m}{11}},m=0,\pm1\cdots\pm5$ are the charges of the Z_{11} group.

To generate masses for most SM fermions at tree level, we use Yukawa interactions involving the scalar triplets η, ρ and their VEVs, as given in Eqs. (4), (5). A convenient approach is adopted in which ρ generates masses for charged leptons and down-type quarks, while η generates masses for up-type quarks. In addition, exotic fermions such as $U_{3L,R}$, $D_{nL,R}$ can also acquire masses at tree level through the VEV of χ, and the gauge singlets N_{aR} may acquire masses through the VEV of the ϕ field. The remaining fermions are the active neutrinos of the SM, which can acquire masses through a type-I seesaw mechanism based on couplings with N_{aR}. To accomplish this, Z_2 is added to the gauge group to eliminate unwanted Yukawa interactions. On the other hand, Z_2 also contributes naturally to PQ symmetry to create a stable axion state [40]. The Z_2 symmetry distinguishes the particles in the model into two classes, even and odd, corresponding to charges of 1 and -1. The odd fields of the Z_2 group are given as [44]

$$(\eta,\rho,u_{aR},d_{aR},l_{aR},N_{aR})\;\to\;-(\eta,\rho,u_{aR},d_{aR},l_{aR},N_{aR}). \tag{7}$$

By introducing the discrete groups discussed above, the full gauge symmetry group of the model is $SU(3)_C\otimes SU(3)_L\otimes U(1)_X\otimes Z_{11}\otimes Z_2$. Under the transformations of this group, the particle assignments are summarized in Table 1.

From Table 1, one can derive the Yukawa interactions of the model, which consist of two parts corresponding to quarks and leptons, where terms that do not preserve the charge of the gauge symmetry group are excluded. The Yukawa couplings invariant under the $SU(3)_C\otimes SU(3)_L\otimes U(1)_X\otimes Z_{11}\otimes Z_2$ symmetry are given by [44]:

$$\begin{aligned}-\mathcal{L}_f^Y&=-\mathcal{L}_q^Y-\mathcal{L}_\ell^Y,\\ -\mathcal{L}_q^Y&=y_1\bar{Q}_{3L}U_{3R}\chi+\sum_{n,p=1}^{2}(y_2)_{np}\,\bar{Q}_{nL}D_{pR}\chi^*\\ &\quad+\sum_{i=1}^{3}(y_3)_{3a}\,\bar{Q}_{3L}u_{aR}\eta+\sum_{n=1}^{2}\sum_{i=1}^{3}(y_4)_{ni}\,\bar{Q}_{nL}d_{iR}\eta^*\\ &\quad+\sum_{i=1}^{3}(y_5)_{3i}\,\bar{Q}_{3L}d_{iR}\rho+\sum_{n=1}^{2}\sum_{i=1}^{3}(y_6)_{ni}\,\bar{Q}_{nL}u_{iR}\rho^*,\end{aligned} \tag{8}$$

$$\begin{aligned}-\mathcal{L}_\ell^Y&=\sum_{i=1}^{3}\sum_{j=1}^{3}g_{ij}\bar{\psi}_{iL}l_{jR}\rho+\sum_{i=1}^{3}\sum_{j=1}^{3}\left(y_\nu^D\right)_{ij}\bar{\psi}_{iL}\eta N_{jR}\\ &\quad+\sum_{i=1}^{3}\sum_{j=1}^{3}(y_N)_{ij}\,\phi\bar{N}_{iR}^C N_{jR}+\text{H.c.}\end{aligned} \tag{9}$$

We can readily see that the Lagrangian in Eqs. (8), (9) is invariant under all elements of the gauge group, including the usual Z_2 group. We emphasize that the transformation under Z_2, as given in Eq. (7), differs from that in Ref. [43], where χ, D_{nR}, U_{3R} are odd. Of course, choosing the action of Z_2 as in Ref. [43] or as in Eq. (7) does not change the Yukawa interactions in Eq. (8), (9). Accordingly, χ couples only to exotic quarks and is responsible for generating masses for particles outside the standard model, except for N_{aR}. The masses of N_{aR} are generated through v_ϕ of the gauge singlet ϕ. Active neutrinos acquire masses via a type-I seesaw mechanism based on the 2nd and 3rd terms of Eq. (8). The mass matrix in the basis $(\nu_{aR},\,N_{aR})$ is

$$\mathrm{M}^\nu=\begin{pmatrix}\mathbf{O}_{3\times3}&M_\nu^D\\(M_\nu^D)^T&M_N\end{pmatrix}, \tag{10}$$

where $M_\nu^D=\frac{y_\nu^D v_\eta}{\sqrt{2}}$ and $M_N=\sqrt{2}y_N v_\phi$ are 3×3 matrices.

Table 1. The $SU(3)_C \otimes SU(3)_L \otimes U(1)_X \otimes Z_{11} \otimes Z_2$ charge assignments of the particle spectrum in the model, with $a = 1,2,3$ and $n = 1,2$.

	Q_{nL}	Q_{3L}	u_{aR}	d_{aR}	U_{3R}	D_{nR}	ψ_{aL}	l_{aR}	N_{aR}	η	χ	ρ	ϕ
$SU(3)_C$	**3**	**3**	**3**	**3**	**3**	**3**	**1**	**1**	**1**	**1**	**1**	**1**	**1**
$SU(3)_L$	$\bar{\mathbf{3}}$	**3**	**1**	**1**	**1**	**1**	**3**	**1**	**1**	**3**	**3**	**3**	**1**
$U(1)_X$	0	$\frac{1}{3}$	$\frac{2}{3}$	$-\frac{1}{3}$	$\frac{2}{3}$	$-\frac{1}{3}$	$-\frac{1}{3}$	-1	0	$-\frac{1}{3}$	$-\frac{1}{3}$	$\frac{2}{3}$	0
Z_{11}	ω_4^{-1}	ω_0	ω_5	ω_2	ω_3	ω_4	ω_1	ω_3	ω_5^{-1}	ω_5^{-1}	ω_3^{-1}	ω_2^{-1}	ω_1^{-1}
Z_2	1	1	-1	-1	1	1	1	-1	-1	-1	1	-1	1

The masses of the active neutrinos are then given by the type-I seesaw mechanism as [47]

$$m_\nu = M_\nu^D M_N^{-1} \left(M_\nu^D\right)^T. \tag{11}$$

Next, we consider the role of the scalar VEVs in generating particle masses in the model. First, the VEV v_ϕ breaks the Z_{11} symmetry, which gives rise to the axion-like particle and inflation. Second, the VEV of χ breaks the flavor symmetry $SU(3)_L$ to the subgroup $SU(2)_L$ and generates masses for the exotic fermions. Third, the two remaining $SU(3)_L$ triplet scalars, η and ρ, generate masses for the SM particles, as in the usual 3-3-1 models. To illustrate this more clearly, we present the following symmetry-breaking scheme:

$$\begin{aligned}
&SU(3)_C \otimes SU(3)_L \otimes U(1)_X \otimes Z(11) \otimes Z_2 \\
&\qquad \downarrow v_\phi \\
&SU(3)_C \otimes SU(3)_L \otimes U(1)_X \otimes Z_2 \\
&\qquad \downarrow v_\chi \\
&SU(3)_C \otimes SU(2)_L \otimes U(1)_Y \otimes Z_2 \\
&\qquad \downarrow v_\eta, v_\rho \\
&SU(3)_C \otimes U(1)_Q \otimes Z_2.
\end{aligned} \tag{12}$$

Clearly, Z_2 is a residual symmetry after the stages of spontaneous symmetry breaking, and it plays a crucial role in identifying stable particles in the model, including potential dark matter candidates.

B. Gauge bosons

We consider the structure of the gauge bosons arising from the nine gauge fields of the electroweak group $SU(3)_L \otimes U(1)_X$, as well as the masses of these bosons derived from the scalar VEVs. They all originate from the scalar kinetic terms, which take the familiar form

$$\mathcal{L}_S = \sum_{S=\chi,\eta,\rho,\phi} (D^\mu S)^\dagger D_\mu S, \tag{13}$$

where D_μ is the covariant derivative, defined as follows:

$$D_\mu \equiv \partial_\mu - \mathrm{i}gT^a W_\mu^a - \mathrm{i}g_X X T^9 B_\mu \equiv \partial_\mu - \mathrm{i}P_\mu, \tag{14}$$

where $T^9 = \frac{I_{3\times3}}{\sqrt{6}}$, with $I_{3\times3}$ denoting the 3×3 identity matrix; W_μ^a $(a = \overline{1,8})$ are the gauge fields of $SU(3)_L$, B_μ is the gauge field of $U(1)_X$, and g and g_X are the gauge couplings of the two groups $SU(3)_L$ and $U(1)_X$, respectively. Furthermore, the matrix $W^a T^a$, where $T^a = \frac{\lambda_a}{2}$ corresponds to the triplet representation, can be written as follows:

$$P_\mu = \frac{g}{2}\begin{pmatrix} W_\mu^3 + \frac{1}{\sqrt{3}}W_\mu^8 + t\sqrt{\frac{2}{3}}XB_\mu & \sqrt{2}W_\mu^+ & \sqrt{2}X_\mu^0 \\ \sqrt{2}W_\mu^- & -W_\mu^3 + \frac{1}{\sqrt{3}}W_\mu^8 + t\sqrt{\frac{2}{3}}XB_\mu & \sqrt{2}Y_\mu^- \\ \sqrt{2}X_\mu^{0*} & \sqrt{2}Y_\mu^+ & -\frac{2}{\sqrt{3}}W_\mu^8 + t\sqrt{\frac{2}{3}}XB_\mu \end{pmatrix}, \tag{15}$$

in which we denote $t = \frac{g_X}{g}$ and define the mass eigenstates of the charged gauge bosons as follows:

$$\begin{aligned}
W_\mu^\pm &= \frac{1}{\sqrt{2}}\left(W_\mu^1 \mp \mathrm{i}W_\mu^2\right), Y_\mu^\pm = \frac{1}{\sqrt{2}}\left(W_\mu^6 \pm \mathrm{i}W_\mu^7\right), \\
X_\mu^0 &= \frac{1}{\sqrt{2}}\left(W_\mu^4 - \mathrm{i}W_\mu^5\right), X_\mu^{0*} = \frac{1}{\sqrt{2}}\left(W_\mu^4 + \mathrm{i}W_\mu^5\right).
\end{aligned} \tag{16}$$

After spontaneous symmetry breaking (SSB), the mass spectrum of the gauge bosons arises from the following kinetic terms:

$$\mathcal{L}_{mass} = \sum_{S=\chi,\eta,\rho} (D^{\mu}\langle S\rangle)^{\dagger}(D_{\mu}\langle S\rangle). \tag{17}$$

The W boson is identical to that in the SM, and its mass is given by

$$m_W^2 = \frac{g^2}{4}(v_\eta^2 + v_\rho^2), \tag{18}$$

while the two *bilepton* gauge bosons (X, Y) acquire masses as follows [48]:

$$m_{X^0}^2 = \frac{g^2}{4}(v_\chi^2 + v_\eta^2), m_Y^2 = \frac{g^2}{4}(v_\chi^2 + v_\rho^2) \tag{19}$$

and their mass splitting from the W boson is [48]

$$|m_Y^2 - m_{X^0}^2| < m_W^2 .$$

From Eq. (18), it follows that

$$v_\eta^2 + v_\rho^2 = v^2 = 246^2\,\mathrm{GeV}^2 . \tag{20}$$

In the basis $(W_\mu^3, W_\mu^8, B_\mu)$, the squared mass mixing matrix of neutral gauge bosons is

$$\mathcal{M}_{NG}^2 = \begin{pmatrix} \frac{g^2}{4}(v_\eta^2 + v_\rho^2) & \frac{g^2}{4\sqrt{3}}(v_\eta^2 - v_\rho^2) & -\frac{gg_X}{6\sqrt{6}}(v_\eta^2 + 2v_\rho^2) \\ & \frac{g^2}{12}(v_\eta^2 + v_\rho^2 + 4v_\chi^2) & \frac{gg_X}{18\sqrt{2}}(2v_\rho^2 + 2v_\chi^2 - v_\eta^2) \\ & & \frac{g_X^2}{54}(v_\eta^2 + 4v_\rho^2 + v_\chi^2) \end{pmatrix}. \tag{21}$$

The matrix $\mathcal{M}_{NG}^2$ has three eigenvalues which belong to photon A and Z, Z' bosons, respectively:

$$\begin{aligned} m_A^2 &= 0, \\ m_Z^2 &= \frac{g^2(9g^2 + 2g_X^2)(v_\eta^2 v_\rho^2 + v_\rho^2 v_\chi^2 + v_\chi^2 v_\eta^2)}{2\left(18g^2(v_\eta^2 + v_\rho^2 + v_\chi^2) + g_X^2(v_\eta^2 + 4v_\rho^2 + v_\chi^2)\right)}, \\ m_{Z'}^2 &= \frac{g^2}{3}(v_\eta^2 + v_\rho^2 + v_\chi^2) + \frac{g_X^2}{54}(v_\eta^2 + 4v_\rho^2 + v_\chi^2) - m_Z^2 . \end{aligned} \tag{22}$$

The physical states of these neutral gauge boson are defined as below:

$$\begin{pmatrix} A_\mu \\ Z_\mu \\ Z'_\mu \end{pmatrix} = \begin{pmatrix} c_{\beta_2} & c_{\beta_1}s_{\beta_2} & s_{\beta_1}s_{\beta_2} \\ -s_{\beta_2} & c_{\beta_1}c_{\beta_2} & c_{\beta_2}s_{\beta_1} \\ 0 & -s_{\beta_1} & c_{\beta_1} \end{pmatrix} \begin{pmatrix} W_\mu^3 \\ W_\mu^8 \\ B_\mu \end{pmatrix}, \tag{23}$$

where, we denote $c_\varphi = \cos\varphi$, $s_\varphi = \sin\varphi$, $t_\varphi = \tan\varphi$ and the mixing angles are given by:

$$\begin{aligned} t_{2\beta_1} &= \frac{6\sqrt{2}t_W(v_\eta^2 - 2v_\rho^2 - 2v_\chi^2)}{2t_W^2(v_\eta^2 + 4v_\rho^2 + v_\chi^2) - 9(v_\eta^2 + v_\rho^2 + 4v_\chi^2)}, \\ t_{2\beta_2} &= -\frac{3\sqrt{6}c_W\left(B\left(v_\eta^2 - v_\rho^2\right) + 2\tan^2\theta_W\left(v_\eta^4 - 3v_\eta^2v_\rho^2 - 5v_\eta^2v_\chi^2 - 7v_\rho^2v_\chi^2 - 4v_\rho^4\right)\right)}{\left(v_\eta^2 - 2v_\rho^2 - 2v_\chi^2\right)\left(A - 2t_W^2\left(v_\eta^2 + 4v_\rho^2 + v_\chi^2\right) + 45\left(v_\eta^2 + v_\rho^2\right) - 36v_\chi^2\right)\sqrt{1 + \frac{\left(Bct_W - 2t_W\left(v_\eta^2 + 4v_\rho^2 + v_\chi^2\right)\right)^2}{72\left(v_\eta^2 - 2v_\rho^2 - v_\chi^2\right)^2}}}, \end{aligned} \tag{24}$$

with $s_w \equiv \sin\theta_W$, θ_W is Weinberg angle as known, and

$$\begin{aligned} A &= \sqrt{\left(2t_W^2\left(v_\eta^2 + 4v_\rho^2 + v_\chi^2\right) + 9\left(v_\eta^2 + v_\rho^2 + 4v_\chi^2\right)\right)^2 - 18(v_\eta^2v_\rho^2 + v_\eta^2v_\chi^2 + v_\rho^2v_\chi^2)}, \\ B &= 9\left(v_\eta^2 + v_\rho^2 + 4v_\chi^2\right) - A . \end{aligned} \tag{25}$$

In the limits $v_\chi \gg v_\eta, v_\rho$, the mixing angle β_2 is very tiny, approximates zero, while the mixing angle β_1 is redefined as:

$$t_{2\beta_1} \approx \frac{6\sqrt{2}t_W}{t_W^2 - 18}. \tag{26}$$

C. The scalar sector

We recall that the scalar self-couplings can include non-Hermitian terms such as $\eta^\dagger\chi$, $\chi^\dagger\eta\phi^*$, and $(\chi^\dagger\eta)^2$, because η and χ have the same quantum numbers, as given in Eq. (4). However, following the assignments introduced in Refs. [40, 44], we eliminate these non-Hermitian terms by extending the gauge group with Z_{11}. Next, we only need to add the Z_2 group to automatically implement the PQ symmetry, thereby ensuring that the axion is naturally stable and light. The action of the Z_{11} and Z_2 symmetries in this work is the same as in 331ALP, as mentioned in Ref. [44]. The Higgs potential then contains only Hermitian terms, as follows [44]:

$$\begin{aligned} V =& \mu_\phi^2\phi^*\phi + \mu_\chi^2\chi^\dagger\chi + \mu_\rho^2\rho^\dagger\rho + \mu_\eta^2\eta^\dagger\eta + \lambda_1(\chi^\dagger\chi)^2 + \lambda_2(\eta^\dagger\eta)^2 \\ &+ \lambda_3(\rho^\dagger\rho)^2 + \lambda_4(\chi^\dagger\chi)(\eta^\dagger\eta) + \lambda_5(\chi^\dagger\chi)(\rho^\dagger\rho) + \lambda_6(\eta^\dagger\eta)(\rho^\dagger\rho) \\ &+ \lambda_7(\chi^\dagger\eta)(\eta^\dagger\chi) + \lambda_8(\chi^\dagger\rho)(\rho^\dagger\chi) + \lambda_9(\eta^\dagger\rho)(\rho^\dagger\eta) \\ &+ \lambda_{10}(\phi^*\phi)^2 + \lambda_{11}(\phi^*\phi)(\chi^\dagger\chi) + \lambda_{12}(\phi^*\phi)(\rho^\dagger\rho) \\ &+ \lambda_{13}(\phi^*\phi)(\eta^\dagger\eta) + \left(\lambda_\phi\epsilon^{ijk}\eta_i\rho_j\chi_k\phi + H.c.\right). \end{aligned} \tag{27}$$

These scalar fields should be expanded around their VEVs as follows:

$$\begin{aligned} \rho_2^0 &= \frac{1}{\sqrt{2}}(v_\rho + R_\rho^2 + \mathrm{i}I_\rho^2), \eta_1^0 = \frac{1}{\sqrt{2}}(v_\eta + R_\eta^1 + \mathrm{i}I_\eta^1), \\ \chi_3^0 &= \frac{1}{\sqrt{2}}(v_\chi + R_\chi^3 + \mathrm{i}I_\chi^3), \phi = \frac{1}{\sqrt{2}}(v_\phi + R_\phi + \mathrm{i}I_\phi). \end{aligned} \tag{28}$$

Substituting (28) into (27) yields the following conditions for the minimum of the potential:

$$\begin{aligned} \mu_\rho^2 + \lambda_3 v_\rho^2 + \frac{\lambda_5}{2}v_\chi^2 + \frac{\lambda_6}{2}v_\eta^2 + \frac{\lambda_{12}}{2}v_\phi^2 + \frac{A}{2v_\rho^2} &= 0, \\ \mu_\eta^2 + \lambda_2 v_\eta^2 + \frac{\lambda_4}{2}v_\chi^2 + \frac{\lambda_6}{2}v_\rho^2 + \frac{\lambda_{13}}{2}v_\phi^2 + \frac{A}{2v_\eta^2} &= 0, \\ \mu_\chi^2 + \lambda_1 v_\chi^2 + \frac{\lambda_4}{2}v_\eta^2 + \frac{\lambda_5}{2}v_\rho^2 + \frac{\lambda_{11}}{2}v_\phi^2 + \frac{A}{2v_\chi^2} &= 0, \\ \mu_\phi^2 + \lambda_{10} v_\phi^2 + \frac{\lambda_{11}}{2}v_\chi^2 + \frac{\lambda_{12}}{2}v_\rho^2 + \frac{\lambda_{13}}{2}v_\eta^2 + \frac{A}{2v_\phi^2} &= 0, \end{aligned} \tag{29}$$

where $\mathcal{A} \equiv \lambda_\phi v_\phi v_\chi v_\eta v_\rho$.

The Higgs potential in Eq. (27) yields the mixing matrix of the charged scalar fields. Diagonalizing it gives the physical states and masses of the charged Higgs bosons. The result is similar to that in Ref. [44]

$$m_{H_1^\pm}^2 = -\frac{v^2}{2}\left(\frac{\mathcal{A}}{v_\rho^2 v_\eta^2} - \lambda_9\right), m_{H_2^\pm}^2 = -\frac{(v_\chi^2 + v_\rho^2)}{2}\left(\frac{\mathcal{A}}{v_\chi^2 v_\rho^2} - \lambda_8\right), \tag{30}$$

with the conditions $\lambda_9 > \lambda_\phi\frac{v_\phi v_\chi}{v_\rho v_\eta}$, $\lambda_8 > \lambda_\phi\frac{v_\phi v_\eta}{v_\chi v_\rho}$, and

$$\begin{aligned} \begin{pmatrix} G_W^\pm \\ H_1^\pm \end{pmatrix} &= \begin{pmatrix} c_\alpha & -s_\alpha \\ s_\alpha & c_\alpha \end{pmatrix}\begin{pmatrix} \rho_1^\pm \\ \eta_2^\pm \end{pmatrix}, \\ \begin{pmatrix} G_Y^\pm \\ H_2^\pm \end{pmatrix} &= \begin{pmatrix} c_{\theta_1} & -s_{\theta_1} \\ s_{\theta_1} & c_{\theta_1} \end{pmatrix}\begin{pmatrix} \chi_2^\pm \\ \rho_3^\pm \end{pmatrix}, \end{aligned} \tag{31}$$

where the mixing angles are defined by $t_\alpha = \frac{v_\eta}{v_\rho}$ and $t_{\theta_1} = \frac{v_\rho}{v_\chi}$, while $G_W^\pm$ and $G_Y^\pm$ are the Goldstone bosons associated with the longitudinal components of $W^\pm$ and $Y^\pm$, respectively.

Next, we consider the mass matrix of the CP-odd scalars. According to Eq. (4), there are six initial pseudoscalars (I_η^3, I_χ^1, I_ϕ, I_χ^3, I_ρ^2, I_η^1). However, they can be separated into two uncoupled bases [40], depending on the scalar VEVs in (28) and the Higgs potential in (27). The first basis is (I_η^3, I_χ^1), corresponding to a 2×2 mass matrix, and the second basis is (I_ϕ, I_χ^3, I_ρ^2, I_η^1), corresponding to a 4×4 mass matrix. The mass matrix in the first basis is easily diagonalized, yielding two physical states, but these are neglected because they are not significantly relevant. In this work, we focus on the 4×4 mass matrix in the (I_ϕ, I_χ^3, I_ρ^2, I_η^1) basis, whose form is [44]

$$M_I^2 = -\frac{\mathcal{A}}{2}\begin{pmatrix} \frac{1}{v_\phi^2} & \frac{1}{v_\phi v_\chi} & \frac{1}{v_\phi v_\rho} & \frac{1}{v_\phi v_\eta} \\ & \frac{1}{v_\chi^2} & \frac{1}{v_\chi v_\rho} & \frac{1}{v_\chi v_\eta} \\ & & \frac{1}{v_\rho^2} & \frac{1}{v_\eta v_\rho} \\ & & & \frac{1}{v_\eta^2} \end{pmatrix}. \tag{32}$$

We can use the Euler method to exactly diagonalize the mass matrix in Eq. (32), as shown in Ref. [44]. The results include two massless states, namely G_Z and $G_{Z'}$, which are absorbed by the Z and Z' bosons, respectively, as well as a massive pseudoscalar and an axion. In a context similar to that discussed in Refs. [40, 49], the model under consideration also possesses an automatic PQ symmetry in the classical Lagrangian, under which we can eliminate the trilinear terms in the Higgs potential. Fortu-

nately, this can be achieved by adding Z_2 to the gauge group, as mentioned above. To obtain a stable axion, we add Z_{11} to the gauge group to prevent the PQ symmetry from being broken by gravitational effects. Interestingly, both Z_{11} and the PQ symmetry are automatically implemented, resulting in a naturally light axion in the model [49]. However, unlike in Refs. [40, 43], the axion state obtained in this work is a combination of $(I_\phi, I^3_\chi, I^2_\rho, I^1_\eta)$. The relationships between the CP-odd scalars in the physical states and the interaction states are given below:

$$a = I_\phi c_{\theta_\phi} - I^3_\chi s_{\theta_3} s_{\theta_\phi} - I^2_\rho s_\alpha c_{\theta_3} s_{\theta_\phi} - I^1_\eta c_\alpha c_{\theta_3} s_{\theta_\phi}, \tag{33}$$

$$G_{Z'} = I^3_\chi c_{\theta_3} - I^2_\rho s_\alpha s_{\theta_3} - I^1_\eta c_\alpha s_{\theta_3}, \tag{34}$$

$$G_Z = I^2_\rho c_\alpha - I^1_\eta s_\alpha, \tag{35}$$

$$A_5 = I_\phi s_{\theta_\phi} + I^3_\chi s_{\theta_3} c_{\theta_\phi} + I^2_\rho s_\alpha c_{\theta_3} c_{\theta_\phi} + I^1_\eta c_\alpha c_{\theta_3} c_{\theta_\phi}, \tag{36}$$

with α given above, the two remaining angles in this sector are:

$$t_{\theta_3} = \frac{v_\eta}{v_\chi}|c_\alpha|, t_{\theta_\phi} = \frac{1}{v_\phi\sqrt{\frac{1}{v^2_\chi}+\frac{1}{v^2_\rho}+\frac{1}{v^2_\eta}}}. \tag{37}$$

Because of the hierarchy of the VEVs, $v_\rho, v_\eta \ll v_\chi \ll v_\phi$, assumed from the outset, the mixing matrix derived in Eq. (36) involves only three angles, α, θ_3, and θ_ϕ, together with one parameter, $\left(\frac{1}{v^2_\phi}+\frac{1}{v^2_\chi}+\frac{1}{v^2_\rho}+\frac{1}{v^2_\eta}\right)$, which appears in the expression for the A_5 mass in Eq. (38). Furthermore, the mass of the new massive CP-odd scalar field A_5 is given by:

$$m^2_{A_5} = -\frac{\mathcal{A}}{2}\left(\frac{1}{v^2_\phi}+\frac{1}{v^2_\chi}+\frac{1}{v^2_\rho}+\frac{1}{v^2_\eta}\right) \approx -\frac{\lambda_\phi v_\phi v_\chi}{s_{2\alpha}}. \tag{38}$$

Equation (38) shows that the values of λ_ϕ should be negative. It is emphasized that both the squared mass mixing matrix in Eq. (32) and the mass of the A_5 field arise from the last term in Eq. (27), which appears only because of the specific discrete symmetry $Z_{11}\otimes Z_2$ imposed on this model from the beginning [40]. Here, the axionlike particle a is massless and is given by the combination of four CP-odd neutral scalar fields, I_ϕ, I^3_χ, I^2_ρ, and I^1_η, as in Eq. (33). Due to $v_\chi \ll v_\phi$, the values of t_{θ_ϕ} as well as s_{θ_ϕ} go to zero, while $c_{\theta_\phi} \simeq 1$, which implies approximately that $a \simeq I_\phi$.

Similarly to the pseudoscalar sector, we also have six original CP-even scalars divided into two uncoupled bases. These two bases are (R^3_η, R^1_χ) and $(R_\phi, R^3_\chi, R^2_\rho, R^1_\eta)$. The mass matrix in the (R^3_η, R^1_χ) basis is easily diagonalized to yield the particle masses because it is a 2×2 matrix. The mass matrix in the remaining basis is 4×4 and is difficult to diagonalize because it has nontrivial eigenvalues. We can use the Hartree-Fock method to diagonalize it, as shown in Ref. [44]. In this way, the original 4×4 matrix is diagonalized successively through three unitary matrices. The three rotation angles characterizing those matrices will be used as dependent parameters in the numerical investigation below. We return to the mass matrix in the $(R^1_\eta, R^2_\rho, R^3_\chi, R_\phi)$ basis, whose form is given in [44]

$$M^2_R = 2\begin{pmatrix} \lambda_2 v^2_\eta - \frac{\mathcal{A}}{4v^2_\eta} & \frac{\lambda_6 v_\eta v_\rho}{4} + \frac{\lambda_\phi v_\chi v_\phi}{4} & \frac{\lambda_4 v_\eta v_\chi}{4} + \frac{\lambda_\phi v_\rho v_\phi}{4} & \frac{\lambda_\phi v_\rho v_\chi}{4} + \frac{\lambda_{13} v_\eta v_\phi}{2} \\ & \lambda_3 v^2_\rho - \frac{\mathcal{A}}{4v^2_\rho} & \frac{\lambda_\phi v_\eta v_\phi}{4} + \frac{\lambda_5 v_\rho v_\chi}{2} & \frac{\lambda\phi v_\eta v_\chi}{4} + \frac{\lambda_{12} v_\rho v_\phi}{2} \\ & & \lambda_1 v^2_\chi - \frac{\mathcal{A}}{4v^2_\chi} & \frac{\lambda\phi v_\eta v_\rho}{4} + \frac{\lambda_{11} v_\chi v_\phi}{2} \\ & & & \lambda_{10} v^2_\phi - \frac{\mathcal{A}}{4v^2_\phi} \end{pmatrix}. \tag{39}$$

The three rotation angles used to diagonalize the matrix M^2_R in Eq. (39) using the Hartree-Fock method are

$$t_{2\alpha_2} = \frac{4c_{\alpha_3} v_\eta v_\rho(\mathcal{A}+\lambda_6 v^2_\eta v^2_\rho)}{\mathcal{A}c^2_{\alpha_3} v^2_\eta - \mathcal{A}v^2_\rho + 4v^2_\eta v^2_\rho(\lambda_2 v^2_\eta - \lambda_3 c^2_{\alpha_3} v^2_\rho)}, \tag{40}$$

$$t_{2\alpha_3} = \frac{4v_\chi\left(\mathcal{A}+2\lambda_5 v^2_\rho v^2_\chi\right)}{c_{\alpha_\phi}\left(\mathcal{A}-4\lambda_1 v^4_\chi\right)^2}, \tag{41}$$

$$t_{2\alpha_\phi} = \frac{\lambda_{11} v_\chi}{\lambda_{10} v_\phi}. \tag{42}$$

After diagonalization of the M_R^2 matrix, four physical CP-even Higgs states are obtained. Two particles have masses at the electroweak scale (h_1, h_2), with the lighter one (h_1) identified as the SM-like Higgs boson. The remaining two particles are expected to be heavier, one with mass proportional to v_χ and the other at the v_ϕ scale. These physical states are

$$h_1 = R_\eta^1 c_{\alpha_2} + R_\rho^2 s_{\alpha_2} c_{\alpha_3} + R_\chi^3 s_{\alpha_2} s_{\alpha_3} c_{\alpha_\phi} - R_\phi s_{\alpha_2} s_{\alpha_3} s_{\alpha_\phi}, \tag{43}$$

$$h_2 = -R_\eta^1 s_{\alpha_2} + R_\rho^2 c_{\alpha_2} c_{\alpha_3} + R_\chi^3 c_{\alpha_2} s_{\alpha_3} c_{\alpha_\phi} - R_\phi c_{\alpha_2} s_{\alpha_3} s_{\alpha_\phi}, \tag{44}$$

$$H_\chi = -R_\rho^2 s_{\alpha_3} + R_\chi^3 c_{\alpha_3} c_{\alpha_\phi} - R_\phi c_{\alpha_3} s_{\alpha_\phi}, \tag{45}$$

$$\Phi = R_\chi^3 s_{\alpha_\phi} + R_\phi c_{\alpha_\phi}. \tag{46}$$

In the limit $v_\phi \gg v_\chi \gg v_\rho, v_\eta$, these physical fields have approximate forms and corresponding masses as follows:

$$\begin{aligned}
&h_1 \approx R_\eta^1 c_{\alpha_2} + R_\rho^2 s_{\alpha_2}, \text{ with } m_{h_1,h_2}^2 \approx \lambda_3 v^2 + \frac{m_{A_5}^2}{2} \mp \sqrt{m_{A_5}^4 + \lambda_3^2\left(v^4 - 3v_\eta^2 v_\rho^2\right) - \frac{\lambda_3 m_{A_5}^2\left(v^4 - 2v_\eta^2 v_\rho^2\right)}{v^2}},\\
&h_2 \approx -R_\eta^1 s_{\alpha_2} + R_\rho^2 c_{\alpha_2},\\
&H_\chi \approx R_\chi^3 c_{\alpha_\phi}, \text{ with } m_{H_\chi}^2 \approx 2\lambda_1 v_\chi^2 + \frac{\lambda_5^2}{2\lambda_1} v_\rho^2,\\
&\Phi \approx R_\phi c_{\alpha_\phi}, \text{ with } m_\Phi = \sqrt{2\lambda_{10} v_\phi}.
\end{aligned} \tag{47}$$

In comparison with the 4×4 mass-mixing matrix of the CP-odd sector, which contains only four parameters and has three massless solutions, the matrix in Eq. (39) has ten parameters and cannot be diagonalized exactly. To address this problem, we use the Hartree-Fock method under the conditions $v_\phi \gg v_\chi \gg v_\rho, v_\eta$, $\lambda_\phi \ll 1$, and $s_{\alpha_3} \approx 0$.

With this VEV hierarchy, the derived matrix contains three angles, α_2, α_3, and α_ϕ, and three parameters associated with the masses of the new fields Φ, H_χ, and h_2. The field H_χ is a heavy scalar boson whose mass should be at the TeV scale. The field Φ, with a heavy mass of order v_ϕ, might be used to explain inflation in the early Universe [44, 46]. We can estimate v_ϕ by preserving the PQ symmetry against the effects of quantum gravity through the addition of the Z_{11} group. Indeed, Z_{11} can eliminate effective operators of the form $\frac{\phi^{N-1}}{M_{Pl}^{N-5}}$ for Z_N, $N = 11$, and make the PQ symmetry an automatic symmetry of the classical Lagrangian. We require that the Peccei-Quinn solution to the strong CP problem be maintained, which means that $\theta \sim \frac{v_\phi^N}{M_{Pl}^{N-4}\Lambda_{\rm QCD}^4} \simeq 10^{-11}$. We recall that the instanton-induced axion mass is given by $m_a \sim \frac{\Lambda_{\rm QCD}^2}{v_\phi}$ and that M_{Pl} is assumed to be 10^{19} GeV [41, 42, 49]; therefore, $v_\phi \sim 10^{11}$ GeV when $N = 11$. Unfortunately, the fields Φ and H_χ are almost devoid of lepton-flavor-violating interactions, based on Eqs. (9), (40), (47). Only two lighter Higgs bosons, denoted by h_1 and h_2, are involved in lepton-flavor-violating processes, which we consider below. Both particles have masses at the electroweak scale, and the lighter one, h_1, is identified with the SM-like Higgs boson.

III. LEPTON FLAVOR VIOLATING DECAY OF CHARGED LEPTON AND CP-EVEN HIGGS BOSONS

In this section, we focus on the lepton-flavor-violating decays $(l_a \to l_b\gamma)$ and $(H \to l_a l_b), H \equiv h_1, h_2$. These channels are closely related because they share a common source of lepton-flavor violation. Based on existing experimental constraints, we identify suitable regions of the model parameter space in which interesting phenomenology and signatures of new physics may arise.

A. Couplings and analytical form related to LFV processes

All lepton-flavor-violating interactions can be derived from the Lagrangian given in Eq. (9). We rewrite them in a convenient form as follows:

$$\begin{aligned}
-\mathcal{L}_{\rm Lepton}^Y &= g_{ab}\overline{\psi}_{aL} l_{bR}\rho + \left(y_\nu^D\right)_{ab}\overline{\psi}_{aL}\eta N_{bR} + (y_N)_{ab}\phi\overline{N}_{aR}^C N_{bR} + \text{H.c.},\\
&= g_{ab}\left(\overline{\nu}_{aL}\rho_1^+ + \overline{l}_{aL}\rho_2^0 + \overline{(\nu_R^c)}_{aL}\rho_3^+\right) l_{bR} + (y_N)_{ab}\phi\overline{N}_{aR}^C N_{bR}\\
&\quad + \left(y_\nu^D\right)_{ab}\left(\overline{\nu}_{aL}\eta_1^0 + \overline{l}_{aL}\eta_2^- + \overline{\nu_{RaL}^c}\eta_3^0\right) N_{bR} + \text{H.c.}
\end{aligned} \tag{48}$$

The lepton mass-mixing matrices are given by

$$-\mathcal{L}^{\rm mass}_{\rm Lepton} = \frac{g_{ab}v_\rho}{\sqrt{2}}\bar{l}_{aL}l_{bR} + \frac{(y_N)_{ab}v_\phi}{\sqrt{2}}\overline{N}^C_{aR}N_{bR} + \frac{(y^D_\nu)_{ab}v_\eta}{\sqrt{2}}\bar{\nu}_{aL}N_{bR} + \text{H.c.}, \tag{49}$$

with the corresponding assignment:

$$m_{l_a} = \frac{g_{ab}v_\rho}{\sqrt{2}}\delta_{ab}, M^D_\nu = y^D_\nu\frac{v_\eta}{\sqrt{2}}, M_N = \sqrt{2}y_N v_\phi, \tag{50}$$

and

$$g_{ab} = \frac{\sqrt{2}m_{l_a}}{v_\rho}\delta_{ab}, y^D_\nu = \frac{\sqrt{2}M^D_\nu}{v_\eta}, y_N = \frac{M_N}{\sqrt{2}v_\phi}. \tag{51}$$

Substituting these expressions into Eq. (48), we obtain the corresponding results for the first and second terms on the right-hand side:

$$\begin{aligned}
g_{ab}\overline{\psi}_{aL}l_{bR}\rho &= g_{ab}\left(\bar{\nu}_{aL}\rho^+_1 + \bar{l}_{aL}\rho^0_2 + \overline{(\nu^c_R)}_{aL}\rho^+_3\right)l_{bR} \\
&= \frac{\sqrt{2}m_{l_a}}{v_\rho}\delta_{ab}\left(\bar{\nu}_{aL}\rho^+_1 + \bar{l}_{aL}\rho^0_2 + \overline{(\nu^c_R)}_{aL}\rho^+_3\right)l_{bR} \\
&\supset \frac{\sqrt{2}m_{l_a}}{v_\rho}\delta_{ab}\left(\bar{\nu}_{aL}l_{bR}s_\alpha H^+_1 + \overline{(\nu^c_R)}_{aL}l_{bR}c_{\theta_1}H^+_2 - \bar{l}_{aL}l_{bR}\left(h_2c_{\alpha_2} + h_1s_{\alpha_2}\right)\right), \\
\left(y^D_\nu\right)_{ab}\overline{\psi}_{aL}\eta N_{bR} &= \frac{\sqrt{2}\left(M^D_\nu\right)_{ab}}{v_\eta}\left(\bar{\nu}_{aL}\eta^0_1 + \bar{l}_{aL}\eta^-_2 + \overline{\nu^c_{RaL}}\eta^0_3\right)N_{bR} \\
&\supset \frac{\sqrt{2}\left(M^D_\nu\right)_{ab}}{v_\eta}\left(-\bar{\nu}_{aL}\left(h_1c_{\alpha_2} - h_2s_{\alpha_2}\right) + \bar{l}_{aL}H^-_1c_\alpha\right)N_{bR}.
\end{aligned} \tag{52}$$

In Eq. (52), we used the supset ($\supset$) notation to indicate the omission of irrelevant interactions that arise when transforming from the interaction basis to the physical basis. The remaining terms are couplings relevant to LFV processes.

In agreement with current experimental observations, charged leptons are assumed not to oscillate, and active neutrinos acquire masses through a type-I seesaw mechanism. We define the transformations between the flavor basis $\{l'_{aL,R}\}$, $\{n'_i\} = \{\nu'_{aL}, (N'_{aR})^C\}$) and the mass basis $\{l_{aL,R}\}$, $\{n_i\} = \{\nu_{aL}, (N_{aR})^C\}$:

$$l'_{aL} = l_{aL},\ l'_{aR} = l_{aR},\ n'_{aL} = U^\nu_{ab}n_{bL},\ n'^C_{aL} = U^{\nu*}_{ab}n^C_{bL},$$
$$\text{where}\quad U^\nu \equiv \begin{pmatrix} O & M^D_\nu \\ (M^D_\nu)^T & M_N \end{pmatrix}, \tag{53}$$

where M^D_ν and M_N have the same form as in Eq. (50).

From the above expansions, we present the lepton-flavor-violating couplings of this model in Table 2,

where

$$\begin{aligned}
\lambda_{h_2H^+_1H^-_1} &= -v\left(-c_{\alpha_2}(\lambda_6+\lambda_9)c^3_\alpha + s_\alpha s_{\alpha_2}(2\lambda_2+\lambda_9)c^2_\alpha - c_{\alpha_2}s^2_\alpha(2\lambda_2+\lambda_9)c_\alpha + s^3_\alpha s_{\alpha_2}(\lambda_6+\lambda_9)\right), \\
\lambda_{h_2H^+_2H^-_2} &= -s_\alpha s_{\alpha_2}v\left(\lambda_6c^2_{\theta_1} + s^2_{\theta_1}\lambda_5\right) + c_\alpha c_{\alpha_2}v\left(2\lambda_2c^2_{\theta_1} + s^2_{\theta_1}(\lambda_5+\lambda_8)\right) + c_{\theta_1}s_{\theta_1}\left(c_{\alpha_2}v_\chi\lambda_8 + s_{\alpha_2}v_\phi\lambda_\phi\right), \\
\lambda_{h_1H^+_1H^-_1} &= v\left(s_{\alpha_2}(\lambda_6+\lambda_9)c^3_\alpha + c_{\alpha_2}s_\alpha(2\lambda_2+\lambda_9)c^2_\alpha + s^2_\alpha s_{\alpha_2}(2\lambda_2+\lambda_9)c_\alpha + c_{\alpha_2}s^3_\alpha(\lambda_6+\lambda_9)\right), \\
\lambda_{h_1H^+_2H^-_2} &= s_{\alpha_2}\left(c_{\theta_1}s_{\theta_1}v_\chi\lambda_8 + c_\alpha v\left(2\lambda_2c^2_{\theta_1} + s^2_{\theta_1}(\lambda_5+\lambda_8)\right)\right) + c_{\alpha_2}\left(s_\alpha v\left(\lambda_6c^2_{\theta_1} + s^2_{\theta_1}\lambda_5\right) - c_{\theta_1}s_{\theta_1}v_\phi\lambda_\phi\right).
\end{aligned} \tag{54}$$

In the framework of 331ALP, there are no trilinear couplings of the form $l_a\bar{l}_b\gamma$ $(a \neq b)$. This can be verified directly from the kinetic term, $\mathcal{L}^{kin}_{Lepton} = -i\bar{\psi}_{aL}\not{D}\psi_{aL}$. Therefore, the decays $(l_a \to l_b\gamma)$ arise only at the loop level. Based on Table 2, we determine that the particles contributing to the loops in these decays can be the following: $(\nu_a, W^\pm)$, $(\nu_a, V^\pm)$, $(\nu_a, H^\pm_{1,2})$, and $(N_a, H^\pm_1)$. The left- and right-handed components of the amplitude for $(l_a \to l_b\gamma)$ are expressed in terms of the PV functions given in Appendix B.

$$\begin{aligned}\mathcal{D}_{(ab)L} &= \mathcal{D}_{(ab)L}\left(m_{\nu_a}, m_W\right) + \mathcal{D}_{(ab)L}\left(m_{\nu_a}, m_V\right) + \mathcal{D}_{(ab)L}\left(m_{\nu_a}, m_{H^{\pm}_{1,2}}\right) + \mathcal{D}_{(ab)L}\left(m_{N_a}, m_{H^{\pm}_1}\right),\\ \mathcal{D}_{(ab)R} &= \mathcal{D}_{(ab)R}\left(m_{\nu_a}, m_W\right) + \mathcal{D}_{(ab)R}\left(m_{\nu_a}, m_V\right) + \mathcal{D}_{(ab)R}\left(m_{\nu_a}, m_{H^{\pm}_{1,2}}\right) + \mathcal{D}_{(ab)R}\left(m_{N_a}, m_{H^{\pm}_1}\right).\end{aligned} \tag{55}$$

The total branching ratios of the cLFV processes can be written based on Refs. [22, 29, 50, 51] in the form:

$$\mathrm{Br}^{\mathrm{Total}}(l_a \to l_b\gamma) \simeq \frac{48\pi^2}{G_F^2}\left(\left|\mathcal{D}_{(ab)R}\right|^2 + \left|\mathcal{D}_{(ab)L}\right|^2\right)\mathrm{Br}(l_a \to l_b\overline{\nu_b}\nu_a), \tag{56}$$

where $G_F = g^2/(4\sqrt{2}m_W^2)$. For decays of different charged leptons, we use the experimental data $\mathrm{Br}(\mu \to e\overline{\nu_e}\nu_\mu) = 100\%$, $\mathrm{Br}(\tau \to e\overline{\nu_e}\nu_\tau) = 17.82\%$, $\mathrm{Br}(\tau \to \mu\overline{\nu_\mu}\nu_\tau) = 17.39\%$ given in Refs.[4, 5, 8].

The couplings in Table 2 are determined by the characteristics of the model under consideration. Therefore, we obtain the following interesting results: *i)* $\bar{N}_a l_b H_2^+ = 0$ implies that diagram 6) receives contributions only from $H_1^{\pm}$, *ii)* N_a does not interact with charged gauge bosons, so diagram 8) gives no contribution in either the h_1 or h_2 case. Therefore, all one-loop Feynman diagrams for the decays $H \to l_a l_b$, $(H \equiv h_1, h_2)$ are shown in Fig. 1, and the corresponding amplitudes are presented in appendix B.

The partial width of $\mathrm{H} \to l_a^{\pm} l_b^{\mp}$ is

$$\Gamma(\mathrm{H} \to l_a l_b) \equiv \Gamma(\mathrm{H} \to l_a^+ l_b^-) + \Gamma(\mathrm{H} \to l_a^- l_b^+) = \frac{m_{\mathrm{H}}}{8\pi}\left(|\Delta_L^{(ab)}|^2 + |\Delta_R^{(ab)}|^2\right). \tag{57}$$

We impose the following conditions on the external momenta: $p_{a,b}^2 = m_{a,b}^2$, $(p_a + p_b)^2 = m_{\mathrm{H}}^2$, and $m_{\mathrm{H}}^2 \gg m_{a,b}^2$. Un-

Table 2. Couplings related to the LFV process in 331ALP. All couplings were considered only in the unitary gauge.

Vertex	Coupling	Vertex	Coupling
$\bar{\nu}_a l_b H_1^+, \bar{l}_b \nu_a H_1^-$	$\mathrm{i}\sqrt{2}U_{ba}^{\nu s}\frac{m_{l_b}}{v_\rho}s_\alpha P_R, \mathrm{i}\sqrt{2}U_{ba}^{\nu}\frac{m_{l_b}}{v_\rho}s_\alpha P_L$	$\bar{\nu}_a l_b H_2^+, \nu_a \bar{l}_b H_2^-$	$\mathrm{i}\sqrt{2}U_{ba}^{\nu s}\frac{m_{l_b}}{v_\rho}c_{\theta_1}P_R, \mathrm{i}\sqrt{2}U_{ba}^{\nu}\frac{m_{l_b}}{v_\rho}c_{\theta_1}P_L$
$\bar{N}_a l_b H_1^+, N_a \bar{l}_b H_1^-$	$\mathrm{i}\sqrt{2}\frac{(M_\nu^D)_{ab}^*}{v_\eta}c_\alpha P_L, \mathrm{i}\sqrt{2}\frac{(M_\nu^D)_{ab}}{v_\eta}c_\alpha P_R$	$\bar{\nu}_a N_b h_2, \bar{\nu}_a N_b h_1$	$-\mathrm{i}\sqrt{2}U_{bc}^{\nu s}\frac{(M_\nu^D)_{ab}}{v_\eta}s_{\alpha_2}P_L, \mathrm{i}\sqrt{2}U_{bc}^{\nu s}\frac{(M_\nu^D)_{ab}}{v_\eta}c_{\alpha_2}P_L$
$\bar{l}_a l_a h_1, \bar{l}_a l_a h_2$	$\frac{\mathrm{i}\sqrt{2}m_{l_a}}{v_\rho}s_{\alpha_2}, \frac{\mathrm{i}\sqrt{2}m_{l_a}}{v_\rho}c_{\alpha_2}$	$\bar{N}_a N_b \phi, H_\chi H_2^+ Y^{\mu-}$	$\frac{(M_N)_{ab}}{\sqrt{2}v_\phi c_{\alpha_\phi}}, \frac{\mathrm{i}g s_{\theta_1}}{2c_{\alpha_\phi}}(p_0 - p_p)$
$\bar{\nu}_a l_b W_\mu^+, \bar{\nu}_a l_b Y_\mu^+$	$\frac{\mathrm{i}g}{\sqrt{2}}U_{ba}^{\nu s}\gamma^\mu P_L$	$\bar{l}_b \nu_a W_\mu^-, \bar{l}_b \nu_a Y Y_\mu^-$	$\frac{\mathrm{i}g}{\sqrt{2}}U_{ab}^{\nu}\gamma^\mu P_L$
$W^{\mu+}W_\mu^- h_1, W^{\mu+}W_\mu^- h_2$	$\frac{\mathrm{i}gm_W}{2}\left(c_\alpha c_{\alpha_2} - s_\alpha s_{\alpha_2}\right), \frac{\mathrm{i}gm_W}{2}\left(c_\alpha s_{\alpha_2} - c_{\alpha_2} s_\alpha\right)$	$Y^{\mu+}Y_\mu^- h_1, Y^{\mu+}Y_\mu^- h_2$	$\frac{\mathrm{i}gm_W}{2}c_\alpha c_{\alpha_2}, \frac{\mathrm{i}gm_W}{2}c_\alpha s_{\alpha_2}$
$h_1 H_1^+ W^{\mu-}, h_2 H_1^+ W^{\mu-}$	$-\frac{\mathrm{i}g}{2}(p_0 - p_p)\left(c_{\alpha_2}s_\alpha + c_\alpha s_{\alpha_2}\right), -\frac{\mathrm{i}g}{2}(p_0 - p_p)\left(c_\alpha c_{\alpha_2} + s_\alpha s_{\alpha_2}\right)$	$h_1 H_2^+ Y^{\mu-}, h_2 H_2^+ Y^{\mu-}$	$-\frac{\mathrm{i}g}{2}(p_0 - p_p)c_{\alpha_2}c_{\theta_1}, -\frac{\mathrm{i}g}{2}(p_0 - p_p)c_{\theta_1}s_{\alpha_2}$
$h_1 H_1^+ H_1^-, h_1 H_2^+ H_2^-$	$-\mathrm{i}\lambda_{h_1 H_1 H_1}, -\mathrm{i}\lambda_{h_1 H_2 H_2}$	$h_2 H_1^+ H_1^-, h_2 H_2^+ H_2^-$	$-\mathrm{i}\lambda_{h_2 H_1 H_1}, -\mathrm{i}\lambda_{h_2 H_2 H_2}$

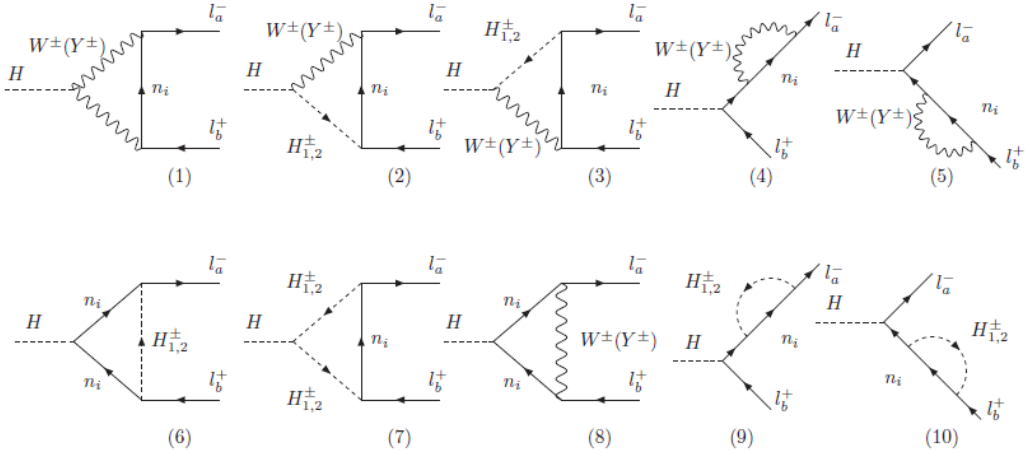


Fig. 1. Feynman diagrams at one-loop order for the decays $H \to l_a l_b$ in the unitary gauge, where $H \equiv \{h_1, h_2\}$.

der these conditions, the branching ratio for the decay $\mathrm{H} \to l_a^{\pm} l_b^{\mp}$ is given by

$$\mathrm{Br}(\mathrm{H} \to l_a l_b) = \Gamma(\mathrm{H} \to l_a l_b)/\Gamma_{\mathrm{H}}^{\mathrm{total}}. \tag{58}$$

We need to determine $\Gamma_{\mathrm{H}}^{\mathrm{total}}$, which can be constrained using current experimental data on the SM Higgs boson [52]. Its main contributions are

$$\begin{aligned}\Gamma_{\mathrm{H}}^{\mathrm{total}} &= \Gamma(\mathrm{H} \to b\bar{b}) + \Gamma(\mathrm{H} \to c\bar{c}) + \Gamma(\mathrm{H} \to \tau\bar{\tau}) \\ &+ \Gamma(\mathrm{H} \to W^* W) + \Gamma(\mathrm{H} \to Z^* Z) \\ &+ \Gamma(\mathrm{H} \to gg) + \Gamma(\mathrm{H} \to \gamma\gamma) + \Gamma(\mathrm{H} \to Z\gamma).\end{aligned} \tag{59}$$

We focus on the SM Higgs boson with a mass of 125.09 GeV. The branching ratios for the channels in Eq. (59) are given in Table 3 [53], and the total decay width (Γ_h^{SM}) is approximately 4.1×10^{-3} GeV [54, 55].

For the CP-even Higgs bosons of the BSM, we can estimate $\Gamma_{\mathrm{H}}^{\mathrm{total}}$ using a method similar to that presented in Ref.[56]. Accordingly, the partial decay width for each channel in Eq. (59) is determined from the branching ratios in Table 3, combined with a comparison to the corresponding quantity in the SM. Applying this procedure to the case $H \equiv h_1$, h_2 in this model, we present the couplings of H to quarks relevant to Eq. (59), based on Eq. (9), in Table 4.

Then, the partial decay widths of the first five channels in Eq. (59) are obtained from a combination of the branching ratios in Table 3 and the couplings in Tables 2 and 4. The last two channels in Eq. (59) are assumed to have the same branching ratios as in the SM. The total decay width is

$$\begin{aligned}\Gamma_{\mathrm{H}}^{\mathrm{total}} \simeq &\sum_f \mathrm{Br}(\mathrm{H} \to f\bar{f}) \left(\frac{g_{Hff}}{g_{hff}^{\mathrm{SM}}}\right)^2 \Gamma_h^{\mathrm{SM}} \\ &+ \sum_G \mathrm{Br}(\mathrm{H} \to G^* G) \left(\frac{g_{HGG}}{g_{hGG}^{SM}}\right)^2 \Gamma_h^{SM} \\ &+ \Gamma(\mathrm{H} \to gg) + \Gamma(\mathrm{H} \to \gamma\gamma) + \Gamma(\mathrm{H} \to Z\gamma),\end{aligned} \tag{60}$$

where $G \equiv W^{\pm}$, Z, $H \equiv h_1$, h_2, and $f \equiv \tau, b, c$.

The last three terms in Eq. (60) are loop-induced decays in the SM. However, since $h_{1,2}$ do not interact with exotic quarks, $\Gamma(\mathrm{H} \to gg) \simeq \Gamma(\mathrm{H} \to \overline{u_3} u_3)$, $u_3 \equiv t$ quark. The remaining two terms are given as

$$\begin{aligned}\Gamma(\mathrm{H} \to \gamma\gamma) &= \mathrm{Br}(\mathrm{H} \to \gamma\gamma)\Gamma_{\mathrm{H}}^{\mathrm{total}}, \\ \Gamma(\mathrm{H} \to Z\gamma) &= \mathrm{Br}(\mathrm{H} \to Z\gamma)\Gamma_{\mathrm{H}}^{\mathrm{total}}.\end{aligned} \tag{61}$$

By substituting Eq. (61) into Eq. (60) and combining the result with Table 3 and Table 4, we can determine the total decay widths of h_1 and h_2. Note that in Eq. (60), $\Gamma_h^{\mathrm{SM}} \simeq 4.1 \times 10^{-3}$ GeV corresponds to $m_h = 125.09$ GeV [54–56], and the current experimental upper bound on $\mathrm{Br}(\mathrm{h} \to \mu\tau)$ is 10^{-3}, as shown in Refs. [4, 5, 8].

B. Numerical results

We use the well-established experimental parameters [4, 8]: the charged-lepton masses $m_e = 5 \times 10^{-4}$ GeV, $m_\mu = 0.105$ GeV, and $m_\tau = 1.776$ GeV; the SM-like Higgs mass $m_h = 125.1$ GeV; the W-boson mass $m_W = 80.385$ GeV; the $SU(2)_L$ gauge coupling $g \simeq 0.651$; and $v = 246$ GeV. The mixing angles are treated as both free and dependent parameters, as specified below, to investigate the numerical behavior of the LFV process. However, this analysis is challenging because of the large number of parameters. This issue can be addressed by choosing t_α and $m_{H_2^{\pm}}$ as free parameters. In particular, t_{α_2} can be expressed as a dependent parameter in terms of t_{α_3}, t_{α_ϕ}, and the VeVs using the relations in Eq. (40).

$$\begin{aligned}t_{\alpha_2} &= \frac{1}{4c_{\alpha_3} v_\eta v_\rho \left(\lambda_6 v_\eta v_\rho + \lambda_\phi v_\chi v_\phi\right)} \left(4\lambda_3 c_{\alpha_3}^2 v_\eta v_\rho^3 - c_{\alpha_3}^2 \lambda_\phi v_\eta^2 v_\chi v_\phi - 4\lambda_3 v_\eta^3 v_\rho + \lambda_\phi v_\rho^2 v_\chi v_\phi \right. \\ &\left. - \frac{1}{2}\sqrt{64 c_{\alpha_3}^2 v_\eta^2 v_\rho^2 \left(\lambda_6 v_\eta v_\rho + \lambda_\phi v_\chi v_\phi\right)^2 + \left(-8\lambda_3 c_{\alpha_3}^2 v_\eta v_\rho^3 + 2c_{\alpha_3}^2 \lambda_\phi v_\eta^2 v_\chi v_\phi + 8\lambda_3 v_\eta^3 v_\rho - 2\lambda_\phi v_\rho^2 v_\chi v_\phi\right)^2}\right), \\ t_{\alpha_3} &= \frac{2\lambda_1 v_\chi^4 c_{\alpha_\phi} + m_{A_5}^2 c_\alpha s_\alpha v_\eta v_\rho c_{\alpha_\phi} + \sqrt{c_{\alpha_\phi}^2 \left(m_{A_5}^2 c_\alpha s_\alpha v_\eta v_\rho + 2\lambda_1 v_\chi^4\right)^2 + 16 v_\rho^2 v_\phi^2 \left(m_{A_5}^2 c_\alpha s_\alpha v_\eta - \lambda_5 v_\rho v_\chi^2\right)^2}}{4 v_\rho v_\phi \left(\lambda_5 v_\rho v_\chi^2 - m_{A_5}^2 c_\alpha s_\alpha v_\eta\right)}, \\ t_{\alpha_\phi} &= \frac{\sqrt{\lambda_{11}^2 v_\chi^2 + \lambda_{10}^2 v_\phi^2} - \lambda_{10} v_\phi}{\lambda_{11} v_\chi},\end{aligned} \tag{62}$$

Table 3. The branching ratios of the SM Higgs boson decays for a mass of 125.09 GeV.

Channel	$\tau\bar{\tau}$	$b\bar{b}$	$c\bar{c}$	W^+W^-	Z^*Z	gg	$\gamma\gamma$	$Z\gamma$
Br(%)	6.32	57.7	2.91	21.5	2.64	8.57	0.228	0.154

Table 4. The coupling of H with fermions.

Couplings	$\bar{\tau}\tau$	$\overline{u_n}u_n$	$\overline{u_3}u_3$	$\overline{d_n}d_n$	$\overline{d_3}d_3$
h_1	$\mathrm{i}\frac{m_\tau}{v_r}s_{\alpha_2}$	$\mathrm{i}\frac{m_{u_n}}{v_r}s_{\alpha_2}$	$-\mathrm{i}\frac{m_{u_3}}{v_e}c_{\alpha_2}$	$-\mathrm{i}\frac{m_{d_n}}{v_e}c_{\alpha_2}$	$\mathrm{i}\frac{m_{d_3}}{v_r}s_{\alpha_2}$
h_2	$-\mathrm{i}\frac{m_\tau}{v_r}c_{\alpha_2}$	$-\mathrm{i}\frac{m_{u_n}}{v_r}c_{\alpha_2}$	$-\mathrm{i}\frac{m_{u_3}}{v_e}s_{\alpha_2}$	$-\mathrm{i}\frac{m_{d_n}}{v_e}s_{\alpha_2}$	$-\mathrm{i}\frac{m_{d_3}}{v_r}c_{\alpha_2}$

where the VEVs are expressed in terms of other parameters, such as the mass of the new charged gauge boson ($m_Y^\pm$) and the mixing angle α ($t_\alpha = \frac{v_\eta}{v_\rho}$). In particular, $v_\chi = \sqrt{\frac{4m_Y^2}{g^2} - v_\rho^2}$, $v_\eta = \frac{vt_a}{\sqrt{t_a^2+1}}$, $v_\rho = \frac{v}{\sqrt{t_a^2+1}}$. The $\sin\phi_i$ and $\cos\phi_i$ functions of arbitrary angles ϕ_i can be related to $\tan\phi_i$ through the formulas $s_{\phi_i} = \frac{t_{\phi_i}}{\sqrt{t_{\phi_i}^2+1}}$, $c_{\phi_i} = \frac{1}{\sqrt{t_{\phi_i}^2+1}}$. Furthermore, the Yukawa couplings and scalar self-coupling constants are chosen to be smaller than $\sqrt{4\pi}$ and 4π, respectively, in order to satisfy the perturbativity limits (Ref. [52]).

Moreover, based on Eqs. (30), (40), the interaction constants are chosen as dependent parameters, whereas the remaining ones are treated as free parameters and must lie within ranges that satisfy the perturbativity limits ($\lambda_i \le 4\pi$). These dependent parameters are listed in Eq. (63).

$$
\begin{aligned}
\lambda_8 &= \frac{2\left(m_{H_2}^2 v_\chi - v^2 m_{A_5}^2 c_\alpha s_\alpha v_\eta\right)}{v^2 v_\rho v_\chi^2},\\
\lambda_9 &= \frac{2\left(m_{H_1}^2 - v^2 m_{A_5}^2 c_\alpha s_\alpha\right)}{v^2 v_\eta v_\rho},\\
\lambda_\phi &= -\frac{2m_{A_5}^2 c_\alpha s_\alpha}{v_\chi v_\phi},\\
\lambda_3 &= \frac{m_{A_5}^2 v_\eta^2 v_\rho^2 - v^4 m_{A_5}^2 + m_h^2 v^4 + \sqrt{\left(m_{A_5}^2\left(v_\eta^2 v_\rho^2 - v^4\right) + m_h^2 v^4\right)^2 + 3v^4 v_\eta^2 v_\rho^2\left(m_h^2 m_{A_5}^2 + \frac{3}{4}m_{A_5}^4 - m_h^4\right)}}{3v^2 v_\eta^2 v_\rho^2}.
\end{aligned}
\tag{63}
$$

To numerically investigate $l_a \to l_b\gamma$ and the LFVHDs, we next consider the parametrization of the neutrino mixing matrix U^ν, starting from the original relation in the seesaw mechanism. It reads:

$$
\hat{M}^\nu \equiv \mathrm{diag}(m_{\nu_1}, m_{\nu_2}, m_{\nu_3}) = U_{\mathrm{PMNS}}^\dagger M_\nu^D M_N^{-1} (M_\nu^D)^T U_{\mathrm{PMNS}}, \tag{64}
$$

$$
U_{\mathrm{PMNS}} \hat{M}^\nu U_{\mathrm{PMNS}}^\dagger = M_\nu^D M_N^{-1} (M_\nu^D)^T. \tag{65}
$$

Using the neutrino oscillation data reported in Refs. [4–6, 8, 57], namely $s_{12}^2 = 0.307$, $s_{23}^2 = 0.558$, $s_{13}^2 = 0.0219$, $\Delta m_{21}^2 = 7.53\times10^{-5}$ eV^2, $\Delta m_{32}^2 = 2.455\times10^{-3}$ eV^2, and choosing the Dirac and Majorana phases of U_{PMNS} in their simplest form (Refs. [16, 51, 58]), we can determine the right-hand side of Eq. (65) in a known form. Furthermore, M_ν^D must be antisymmetric; therefore, it contains only six unknowns. Together with M_N in diagonal form, this gives three additional unknowns. Hence, there are nine unknowns in total on the right-hand side, so Eq. (65) can be solved. This means that we have successfully parametrized U^ν.

We investigate the numerical results for $l_a \to l_b\gamma$ in the parameter space $10^{-3} \le t_\alpha \le 10^3$ and $300 \le m_{H_2}^\pm \le 5\times10^3$ GeV. We find that $\tau \to e\gamma$ is always below the experimental limit (4.4×10^{-8}). The region of parameter space exceeding the upper limit for $\tau \to \mu\gamma$ is indicated in green, with pink dashed lines corresponding to $\mathrm{Br}(\tau \to \mu\gamma) = 3.3\times10^{-8}$ and 15×10^{-8}. Meanwhile, the yellow and blue markers represent the parameter space in which $\mathrm{Br}(\mu \to e\gamma)$ takes values above the upper bound. The curves corresponding to $\mathrm{Br}(\mu \to e\gamma) = 4.2\times10^{-13}$ and

10×10^{-13} can also be found there. Therefore, the region allowed by the experimental constraints on $l_a \to l_b\gamma$ decays is the uncolored part in Fig. 2.

Based on the analytical expressions for the amplitudes given in appendix B, we investigate the values of $\mathrm{Br}(h_1 \to \mu\tau)$ and $\mathrm{Br}(h_2 \to \mu\tau)$, which are shown in Fig. 3. We observe that most of the values of $\mathrm{Br}(h_1 \to \mu\tau)$ in the left panel and $\mathrm{Br}(h_2 \to \mu\tau)$ in the right panel lie within the current experimental limits ($\lesssim 10^{-3}$).

To illustrate this, we present the signals of $\mathrm{Br}(h_1 \to \mu\tau)$ and $\mathrm{Br}(h_2 \to \mu\tau)$ in the allowed parameter-space region in Fig. 3. In the left panel of Fig. 3, $\mathrm{Br}(h_1 \to \mu\tau)$ can reach values of 3.4×10^{-6} and 6.7×10^{-6}, while in the right panel, $\mathrm{Br}(h_2 \to \mu\tau)$ can reach values of 9.1×10^{-5} and 5.6×10^{-5}. All of these values satisfy the current experimental limits.

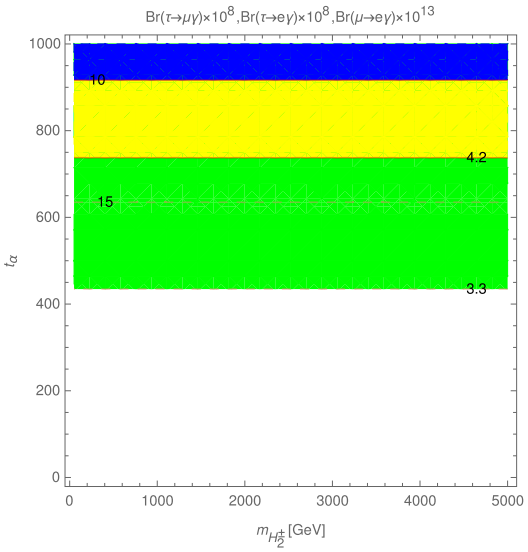


Fig. 2. (color online) Contour plots of $l_a \to l_b\gamma$ decays in the plane of $(t_\alpha, m_{H_2^\pm})$.

Next, we predict the mass of the new CP-even Higgs boson based on gluon-gluon fusion at the LHC and the CMS data analysis. The Higgs-boson production signal in proton-proton collisions is modeled under the assumption of a narrow Higgs-boson width [59]. In this case, the partons can be gluons or quarks [60, 61]. Therefore, the hadronic cross section depends on the parton luminosity and the partonic cross section as follows [60, 61]

$$\sigma(pp \to H) = \sum_{p_i,p_j=\{g,\,q\}} \mathcal{L}_{p_ip_j}\left(m_H^2\right)\hat{\sigma}\left(p_ip_j \to H\right), \tag{66}$$

where g and q denote gluons and quarks, respectively.

As shown in Eq. (66), Higgs boson production in proton-proton collisions at the LHC involves partons, namely gluons and quarks. However, because of their relatively large masses, the densities of quarks inside the proton are significantly lower than that of gluons. Consequently, the gluon parton distribution plays the dominant role in Higgs production, with the gluons eventually coupling through a quark loop. Therefore, we approximate the hadronic cross section by considering only gluon-initiated partons, which takes the form [62, 63]

$$\sigma(pp \to H) \simeq \sigma(gg \to H) = \mathcal{L}_{gg}\left(m_H^2\right)\hat{\sigma}(gg \to H). \tag{67}$$

The parton luminosity is related to the parton distribution function as

$$\mathcal{L}_{gg}\left(m_H^2\right) = \int_{\frac{m_H^2}{s}}^1 \frac{\mathrm{d}x_1}{x_1}\int_{x_1}^1 \frac{\mathrm{d}x_2}{x_2}\left[F_g\left(\frac{x_1}{x_2}, m_H^2\right)F_g\left(x_2, m_H^2\right)\right] \times\delta\left(x_1x_2 - \frac{m_H^2}{s}\right), \tag{68}$$

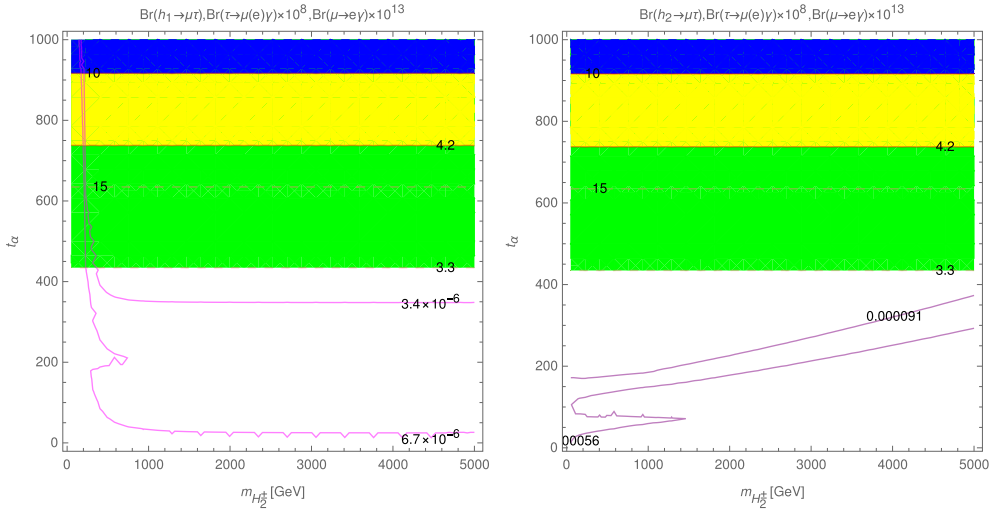


Fig. 3. (color online) Plots of $\mathrm{Br}(h_1 \to \mu\tau)$ (left panel) and $\mathrm{Br}(h_2 \to \mu\tau)$ (right panel) in the $(t_\alpha, m_{H_2^\pm})$ plane.

where $F_g\left(x,m_H^2\right)$ is the gluon parton distribution function, $\sqrt{s}$ is the center-of-mass energy of the collider, and $\hat{\sigma}$ is the partonic cross section, expanded in terms of the strong coupling constant (α_s), as follows Refs. [60, 61]:

$$\hat{\sigma}(gg\to H)=\alpha_s^2\left[\hat{\sigma}^{(0)}(gg\to H)+\alpha_s\hat{\sigma}^{(1)}(gg\to H)+...\right]. \tag{69}$$

Loop corrections involving intermediate quarks are the primary source of Higgs boson production via gluon-gluon fusion. However, the t-quark provides the dominant contribution to this process, because the Higgs boson couples about 35 times more strongly to the t-quark than to the next-heaviest fermion, the b-quark. Consequently, the other contributions can be neglected, and only the t-quark contribution needs to be considered. Thus, the leading-order approximation in Eq.(69) is expressed as follows [60, 64]:

$$\hat{\sigma}^{(0)}(gg\to H)=\frac{9G_{\rm F}m_H^2\zeta^2}{1152\sqrt{2}\pi}\left|1+(1-\zeta)f(\zeta)\right|^2, \tag{70}$$

where $G_{\rm F}$ is the Fermi constant, $\zeta=\dfrac{4m_t^2}{m_H^2}$, m_t is t-quark mass and

$$f(\zeta)=\begin{cases}\arcsin^2\dfrac{1}{\sqrt{\zeta}}, & \zeta\geq 1,\\ \dfrac{1}{2}\left[\ln\dfrac{1-\sqrt{1-\zeta}}{1+\sqrt{1-\zeta}}-{\rm i}\pi\right]^2, & \zeta<1.\end{cases} \tag{71}$$

For dilepton decays, if the decay width is assumed to be very narrow, the cross section of these processes can be approximated as

$$\sigma\left(gg\to H\to\bar{l}_il_j\right)\simeq\sigma(gg\to H)\times{\rm Br}\left(H\to\bar{l}_il_j\right). \tag{72}$$

By analyzing data at a center-of-mass energy of 13 TeV and an integrated luminosity of 35.9 fb^{-1}, CMS has shown that $\sigma(gg\to H)\times{\rm Br}(H\to\mu\tau)$ can range from 51.9 (57.4) fb to 1.6 (2.1) fb at the 95% confidence level [38]. To optimize the analysis of the experimental data, CMS divided the mass range into two regions: a low-mass region of 200–450 GeV and a high-mass region of 450–900 GeV.

As results, we present the combined processes $\sigma(gg\to H)\times{\rm Br}(H\to\mu\tau_h)$ and $\sigma(gg\to H)\times{\rm Br}(H\to\mu\tau_e)$ at 95% CL as the green and cyan lines, respectively, in Fig. 4. The dotted black line represents the boundary between the two mass scales.

To predict the masses of the new CP-even Higgs bosons, h_2, the parton distribution functions are chosen in a non-relativistic form (Breit-Wigner distribution functions), and the partonic cross section is approximated at leading order. For simplicity, $\hat{\sigma}(gg\to H)\sim\dfrac{G_Fm_H^2\zeta^2}{\sqrt{2}\pi}|1+(1-\zeta)f(\zeta)|^2$. Therefore, we investigate the signal $\sigma\left(gg\to h_2^0\right)\times{\rm Br}\left(h_2^0\to\mu\tau\right)$, shown as the magenta line in Fig. 4, and the mass of h_2 is predicted to be greater than 630 GeV.

IV. Z' BOSON

In 331ALP, the heavier neutral gauge boson, Z', has the mass and physical state given by Eq.(22) in section II. The interaction of Z' with fermions originates from the kinetic term of the spinor fields and has the following form:

$$\mathcal{L}_{NC}^{Z'}\supset\overline{f}\gamma^\mu\left(g_V^{Z'}(f)+g_A^{Z'}(f)\gamma^5\right)fZ'_\mu, \tag{73}$$

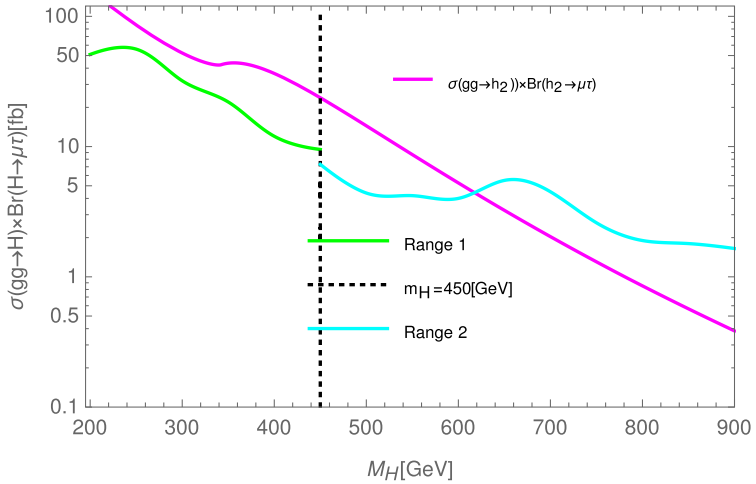


Fig. 4. (color online) Plots of $\sigma(gg\to h_2)\times{\rm Br}(h_2\to\mu\tau)$ (magenta line) as functions of M_H are shown, while the green and cyan lines represent the CMS observations for the combined decay modes of $H\to\mu\tau$ (based on Ref. [38]) in the low- and high-mass ranges, respectively.

where $g_V^{Z'}$ and $g_A^{Z'}$ are given in Table 5.

We also use the kinetic terms of the scalar fields, such as Eq. (13), to derive the non-zero couplings of Z' to gauge and Higgs bosons, as shown in Table 6.

The LHC dilepton measurements at $\sqrt{s} = 13$ TeV indicate that the cross section for the Z'-mediated process is given by the product of the hadronic cross section and the branching ratio [39]

$$\sigma\left(pp \to Z' \to \bar{l}l\right) \simeq \sum_q \int_\tau^1 \frac{\mathrm{d}x_1}{x_1} \int_\tau^1 \frac{\mathrm{d}x_2}{x_2} \xi_q\left(\frac{x_1}{x_2}, m_Z^2\right) \bar{\xi}_q\left(x_2, m_Z^2\right) \hat{\sigma}\left(\bar{q}qi \to Z\right) \times \mathrm{Br}\left(Z \to \bar{l}l\right), \tag{74}$$

where ξ_q and $\bar{\xi}_q$ denote the parton distribution functions of quarks and antiquarks, respectively. The partonic cross section and branching ratio are given by:

$$\begin{aligned} \hat{\sigma}\left(\bar{q}q \to Z'\right) &= \frac{\pi g^2}{3c_W^2} \sum_i \left[\left(g_V^{Z'}\left(q_i\right)\right)^2 + \left(g_A^{Z'}\left(q_i\right)\right)^2\right], \\ \mathrm{Br}\left(Z' \to \bar{l}l\right) &= \frac{\Gamma\left(Z' \to \bar{l}l\right)}{\Gamma_{Z'}^{\mathrm{tot}}}, \end{aligned} \tag{75}$$

where the final-state particles in the decay channel are dileptons. The corresponding decay width is given by Eq. (76), while the total decay width must also include the gauge and Higgs boson contributions, denoted by G and H, respectively, as listed in Eq. (77).

$$\Gamma\left(Z' \to \bar{l}l\right) \simeq \frac{m_{Z'}}{12\pi} \frac{\pi g^2}{c_W^2} \sum_{e,\mu,\tau,\nu,N_a} \sqrt{1 - \frac{4m_l^2}{m_{Z'}^2}} \left[\left(g_V^{Z'}(l)\right)^2 \times \left(1 + \frac{2m_l^2}{m_{Z'}^2}\right) + \left(g_A^{Z'}(l)\right)^2 \left(1 - \frac{4m_l^2}{m_{Z'}^2}\right)\right], \tag{76}$$

$$\Gamma_{Z'}^{\mathrm{tot}} \simeq \Gamma\left(Z' \to \bar{f}f\right) + \Gamma\left(Z' \to H^* H\right) + \Gamma\left(Z' \to GH\right) + \Gamma\left(Z' \to G^* G\right). \tag{77}$$

Because Z and Z' do not mix, as shown in Eq. (22), $\Gamma(Z' \to W^+W^-)$ vanishes, according to Ref. [66]. Furthermore, since $m_X > m_{Z'}/2$, $\Gamma(Z' \to X^* X,\ X \equiv V^\pm, X^{0*}, X^0$ also does not contribute to the total width of Z'. The remaining components are given as follows [45, 65, 66]:

$$\Gamma\left(Z' \to \bar{f}f\right) \simeq \frac{m_{Z'}}{12\pi} \frac{\pi g^2}{c_W^2} \sum_f N_C(f) \sqrt{1 - \frac{4m_f^2}{m_{Z'}^2}} \left[\left(g_V^{Z'}(f)\right)^2 \times \left(1 + \frac{2m_f^2}{m_{Z'}^2}\right) + \left(g_A^{Z'}(f)\right)^2 \left(1 - \frac{4m_f^2}{m_{Z'}^2}\right)\right]. \tag{78}$$

$$\Gamma\left(Z' \to H^* H\right) \simeq \frac{m_{Z'}}{48\pi} \sum_H g_{Z'HH}^2 \left(1 - \frac{4m_H^2}{m_{Z'}^2}\right)^{3/2}. \tag{79}$$

Table 5. The couplings of Z' to fermions are expressed in terms of the angle β_1, defined in Eq. (24), and $t = \frac{g_X}{g} = \frac{3\sqrt{2}t_W}{\sqrt{3 - t_W^2}}$, as shown in Ref. [65].

f	ν_e, ν_μ, ν_τ	e, μ, τ	u, c	d, s	t	b	U_3	D_n
$g_V^{Z'}$	$g\left(\frac{s_{\beta_1}}{4\sqrt{3}} - \frac{2tc_{\beta_1}}{3\sqrt{6}}\right)$	$g\left(\frac{s_{\beta_1}}{4\sqrt{3}} - \frac{2tc_{\beta_1}}{3\sqrt{6}}\right)$	$g\left(\frac{s_{\beta_1}}{4\sqrt{3}} + \frac{tc_{\beta_1}}{3\sqrt{6}}\right)$	$g\left(\frac{s_{\beta_1}}{4\sqrt{3}} - \frac{tc_{\beta_1}}{6\sqrt{6}}\right)$	$g\left(\frac{s_{\beta_1}}{4\sqrt{3}} + \frac{tc_{\beta_1}}{2\sqrt{6}}\right)$	$\frac{gs_{\beta_1}}{4\sqrt{3}}$	$g\left(-\frac{s_{\beta_1}}{2\sqrt{3}} + \frac{tc_{\beta_1}}{3\sqrt{6}}\right)$	$-\frac{gs_{\beta_1}}{2\sqrt{3}}$
$g_A^{Z'}$	$g\left(\frac{s_{\beta_1}}{4\sqrt{3}} - \frac{tc_{\beta_1}}{3\sqrt{6}}\right)$	$g\left(\frac{s_{\beta_1}}{4\sqrt{3}} - \frac{tc_{\beta_1}}{3\sqrt{6}}\right)$	$g\left(\frac{s_{\beta_1}}{4\sqrt{3}} + \frac{tc_{\beta_1}}{3\sqrt{6}}\right)$	$g\left(\frac{s_{\beta_1}}{4\sqrt{3}} - \frac{tc_{\beta_1}}{6\sqrt{6}}\right)$	$g\left(\frac{s_{\beta_1}}{4\sqrt{3}} + \frac{tc_{\beta_1}}{6\sqrt{6}}\right)$	$g\left(\frac{s_{\beta_1}}{4\sqrt{3}} - \frac{tc_{\beta_1}}{3\sqrt{6}}\right)$	$g\left(-\frac{s_{\beta_1}}{2\sqrt{3}} + \frac{tc_{\beta_1}}{3\sqrt{6}}\right)$	$g\left(-\frac{s_{\beta_1}}{2\sqrt{3}} - \frac{tc_{\beta_1}}{3\sqrt{6}}\right)$

Table 6. The couplings of Z' to charged and gauge bosons.

Vertex	Coupling
$Z' H_1^+ H_1^-$	$-\frac{2g\left(c_\alpha^2\left(\sqrt{4c_W^2-1}c_{\beta_1}\left(\sqrt{3}-3s_{\beta_1}\right)-6s_W s_{\beta_1}s_{\beta_2}\right)-s_\alpha^2\left(\sqrt{4c_W^2-1}c_{\beta_1}\left(3s_{\beta_1}+\sqrt{3}\right)+12s_W s_{\beta_1}s_{\beta_2}\right)\right)}{6\sqrt{4c_W^2-1}}$
$Z' H_2^+ H_2^-$	$-\frac{2g\left(2\left(\sqrt{12c_W^2-3}c_{\beta_1}-6s_W s_{\beta_1}s_{\beta_2}\right)c_{\theta_1}^2+\left(\sqrt{4c_W^2-1}c_{\beta_1}\left(\sqrt{3}-3s_{\beta_1}\right)-6s_W s_{\beta_1}s_{\beta_2}\right)s_{\theta_1}^2\right)}{6\sqrt{4c_W^2-1}}$
$Z' H_1^+ W^-$	$\frac{1}{3}gm_W c_\alpha s_\alpha\left(\sqrt{3}c_{\beta_1}+\frac{3s_W s_{\beta_1}s_{\beta_2}}{\sqrt{4c_W^2-1}}\right)$
$Z' H_2^+ Y^-$	$-\frac{g^2\left(c_\alpha c_{\theta_1}\left(\sqrt{4c_W^2-1}c_{\beta_1}\left(3s_{\beta_1}+\sqrt{3}\right)-24s_W s_{\beta_1}s_{\beta_2}\right)v+\left(\sqrt{4c_W^2-1}c_{\beta_1}\left(3s_{\beta_1}+\sqrt{3}\right)+12s_W s_{\beta_1}s_{\beta_2}\right)s_{\theta_1}v_\chi\right)}{12\sqrt{4c_W^2-1}}$

$$\Gamma(Z' \to GH) \simeq \sum_{G,H} \frac{g^2_{Z'GH}}{24\pi} \frac{E^2 - m_G^2}{m_{Z'}^2} \left(2 + \frac{E^2}{m_G^2}\right), \tag{80}$$

where $E = \dfrac{m_{Z'}^2 + m_G^2 - m_H^2}{2m_{Z'}}$ denotes the energy of the final-state gauge boson, and the corresponding factors are taken from Tables 5 and 6.

Based on the analytical expressions in Eqs. (74), (75) and the known data given in Sec. IV, we show the dependence of $\sigma\left(pp \to Z' \to \bar{l}l\right)$ on $m_{Z'}$ as the blue line in Fig. 5. The red line depicts the upper limits on the dilepton production cross section reported by ATLAS at an integrated luminosity of 139 fb^{-1} [7], while the black line is based on the 95% CL upper bound given by CMS at $\sqrt{s} = 13$ TeV [39]. Therefore, to satisfy these constraints, we obtain $m_{Z'} \geqslant 5.1$ TeV; of course, for masses below this value, Z' is excluded. The lower bound on the Z' mass obtained in this work is highly consistent with non-supersymmetric models, such as Z'_ψ in grand unified theories based on the E_6 gauge group or Z'_{SSM} in the generalized sequential model [7, 39]. However, a major difference arises in supersymmetric models, where the lower bound on $m_{Z'}$, as mentioned above, is significantly smaller [67, 68].

V. DARK MATTER

From the symmetry-breaking scheme in (12), we see that Z_2 is the residual symmetry of the model; therefore, **odd**-Z_2 particles can be considered dark matter candidates. These include $\eta, \rho, u_{aR}, d_{nR}, l_{aR}, N_{aR}$, according to (7). However, η and ρ directly break the electroweak scale, and u_{aR}, d_{nR}, l_{aR} are components of ordinary matter; thus, only N_{aR} remains the most suitable dark matter candidate in the model.

Among N_{aR}, we assume that N_{1R} is the lightest. Therefore, N_{1R} is identified as dark matter, and pairs of N_{1R} annihilate into SM particles in the early universe. Because N_{1R} interacts directly only with Φ according to Eq. (9), and Φ can couple to SM particles as in Eq. (27), the dominant contribution to dark matter annihilation mainly arises from s-channel exchange diagrams mediated by Φ. The corresponding diagram is shown in Fig. 6. Although Φ mixes with R_χ and R_ϕ, and can therefore interact with fermions according to Eq. (46), the mixing angles are very small, as shown in Eq. (40). Therefore, the SM products of the dark matter pair annihilation channel do not include fermions, but only gauge bosons. This implies that $N^C_{1R}N_{1R} \to h_1 h_1, ZZ$. Hence, the product of the annihilation cross section of the dark matter pair and the relative velocity is approximately [39, 69]

$$\langle \sigma v_{\rm rel} \rangle_{N^C_{1R}N_{1R} \to \rm all} = 2\sigma_\Lambda F_{-4}(x_f) \simeq \frac{3}{x_f}\sigma_\Lambda \simeq \frac{3m^2_{N_{1R}}}{4\pi x_f} \times \left\{ \frac{\left(g_{\Phi N^C_{1R}N_{1R}}\right)^2}{4m^2_{N_{1R}} - m^2_\Phi} \times \left[(g_{\Phi ZZ})^2 + \left(g_{\Phi h_1 h_1}\right)^2\right] \right\}, \tag{81}$$

where $x_f \simeq 20.25$ [70] and $g_{\Phi N^C_{1R}N_{1R}} = (y_N)_{11}$, whereas $g_{\Phi ZZ} = 0$ and $g_{\Phi h_1 h_1} = \dfrac{v_\phi}{2\sqrt{2}}\left(\lambda_{12}s^2_{\alpha_2} + \lambda_{13}c^2_{\alpha_2}\right)$ are determined from Eq. (13) and Eq. (27), respectively.

We employed the dark matter relic abundance given in Ref. [71]:

$$\Omega_{\rm DM}h^2 \simeq \frac{0.1 \text{ pb}}{\langle \sigma v_{\rm rel} \rangle_{N^C_{1R}N_{1R} \to \rm all}}. \tag{82}$$

We represent the dark matter relic density, $0.1 \leq \Omega_{\rm DM}h^2 \leq$

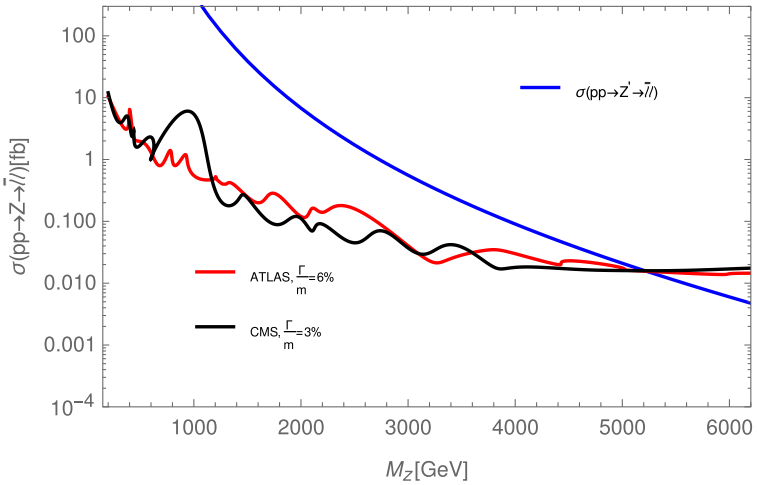


Fig. 5. (color online) The dependence of $\sigma\left(pp \to Z' \to \bar{l}l\right)$ on M_Z is shown by the blue line. The red line represents the ATLAS upper limits on the cross section for $\Gamma/m = 6\%$ [7]. The black line represents the CMS upper limits on the cross section for $\Gamma/m = 3\%$ at 95% CL [39].

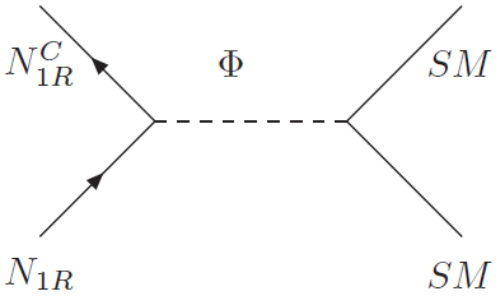


Fig. 6. Dominant contributions to dark matter annihilation.

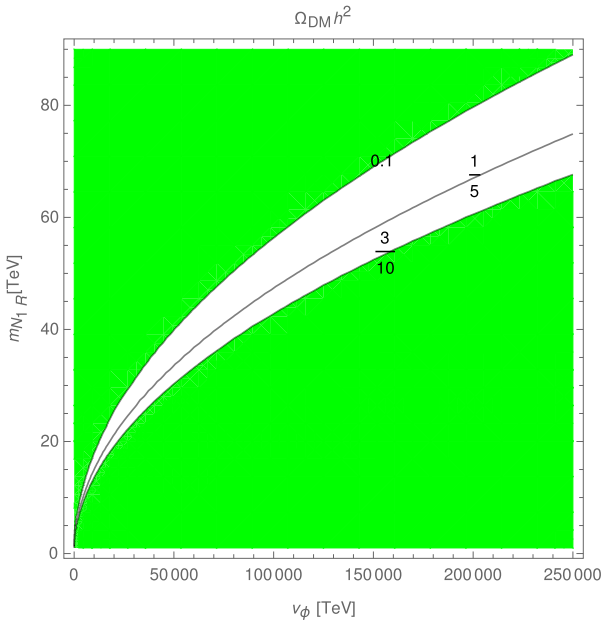


Fig. 7. (color online) Contours of the dark matter relic density in the $(v_\Phi, m_{N_{1R}})$ plane.

0.3 [72], in the $(v_\Phi, m_{N_{1R}})$ plane, as shown in Fig. 7. We recall that, for the PQ symmetry not to be broken by quantum gravity effects and to ensure the emergence of a naturally light, stable axion, $v_\phi \simeq 10^{11}$ GeV (as mentioned in Sec. II). Therefore, v_ϕ is taken to be the axion-breaking scale in the model. As a result, in Fig. 7, the colorless region corresponds to the parameter space consistent with current observations, in which there is a relationship between the dark matter mass and the axion-breaking scale.

VI. CONCLUSIONS

In the 3-3-1 model with axionlike particles, we identify the region of parameter space in which both cLFV and LFVHD constraints satisfy the experimental limits. In these allowed regions, $\mathrm{Br}(h_1 \to \mu\tau)$ is of the order of 10^{-6}, while $\mathrm{Br}(h_2 \to \mu\tau)$ reaches approximately 10^{-5}. Based on gluon-gluon fusion at the LHC, we investigate the signal cross sections in the allowed parameter space and provide predictions for $m_{h_2} \geq 630$ GeV. Based on searches for high-mass dilepton resonances at ATLAS and CMS, we use the numerical result for $\sigma\left(pp \to Z' \to \bar{l}l\right)$ and show that the Z'-boson mass satisfies $m_{Z'} \geq 5.1$ TeV. The hypothesis of the existence of a residual Z_2 symmetry after the stages of spontaneous symmetry breaking implies that only N_{aR} can be dark matter candidates among the odd-Z_2 particles. By investigating the dark matter relic density within experimentally allowed limits, we also establish a relationship between the dark matter mass and the axion breaking scale.

ACKNOWLEDGMENTS

H.T. Hung would like to thank A.V. Bednyakov for his helpful comments on improving this article.

APPENDIX A. MASTER INTEGRALS

In this section, we use the Passarino–Veltman (PV) functions introduced in Ref. [73] to derive the one-loop contributions of the Feynman diagrams in Fig. 1. Introducing the denominators $D_0 = k^2 - M_0^2 + \mathrm{i}\delta$, $D_1 = (k-p_1)^2 - M_1^2 + \mathrm{i}\delta$, and $D_2 = (k+p_2)^2 - M_2^2 + \mathrm{i}\delta$, where δ is an infinitesimally small positive real quantity, we obtain:

$$
\begin{aligned}
&A_0(M_n) \equiv \frac{(2\pi\mu)^{4-D}}{\mathrm{i}\pi^2}\int\frac{d^Dk}{D_n}, B_0^{(12)} \equiv \frac{(2\pi\mu)^{4-D}}{\mathrm{i}\pi^2}\int\frac{d^Dk}{D_1D_2},\\
&B_0^{(1)} \equiv \frac{(2\pi\mu)^{4-D}}{\mathrm{i}\pi^2}\int\frac{d^Dk}{D_0D_1}, B_0^{(2)} \equiv \frac{(2\pi\mu)^{4-D}}{\mathrm{i}\pi^2}\int\frac{d^Dk}{D_0D_2},\\
&C_0 \equiv C_0(M_0,M_1,M_2) = \frac{1}{\mathrm{i}\pi^2}\int\frac{d^4k}{D_0D_1D_2},
\end{aligned}
\tag{A1}
$$

where $n = 1,2$, $D = 4-2\epsilon \leq 4$ is the dimension of the integral, while M_0, M_1, M_2 denote the masses of the virtual particles in the loops. We also assume that $p_1^2 = m_1^2$ and $p_2^2 = m_2^2$ for the external particles. The tensor integrals are

$$
\begin{aligned}
&A^\mu(p_n;M_n) = -\frac{\mathrm{i}(2\pi\mu)^{4-D}}{\pi^2}\int\frac{k^\mu\times d^Dk}{D_n} = A_0(M_n)p_n^\mu,\\
&B^\mu(p_n;M_0,M_n) = -\frac{\mathrm{i}(2\pi\mu)^{4-D}}{\mathrm{i}\pi^2}\int\frac{k^\mu\times d^Dk}{D_0D_n} \equiv B_1^{(n)}p_n^\mu,\\
&B^\mu(p_1,p_2;M_1,M_2) = -\frac{\mathrm{i}(2\pi\mu)^{4-D}}{i\pi^2}\int\frac{k^\mu\times d^Dk}{D_1D_2} \equiv B_1^{(12)}p_1^\mu + B_2^{(12)}p_2^\mu,\\
&C^\mu(M_0,M_1,M_2) = -\frac{\mathrm{i}}{\pi^2}\int\frac{k^\mu\times d^4k}{D_0D_1D_2} \equiv C_1p_1^\mu + C_2p_2^\mu,\\
&C^{\mu\nu}(M_0,M_1,M_2) = -\frac{\mathrm{i}}{\pi^2}\int\frac{k^\mu k^\nu\times d^4k}{D_0D_1D_2} \equiv C_{00}g^{\mu\nu} + C_{11}p_1^\mu p_1^\nu\\
&\qquad + C_{12}p_1^\mu p_2^\nu + C_{21}p_2^\mu p_1^\nu + C_{22}p_2^\mu p_2^\nu,
\end{aligned}
\tag{A2}
$$

where A_0, $B_{0,1}^{(n)}$, $B_n^{(12)}$, and $C_{0,n}, C_{mn}$ are PV functions. It

should be noted that only A_0, $B^{(n)}_{0,1}$, and $B^{(12)}_n$ contain divergences, which are denoted by

$$\Delta_\epsilon \equiv \frac{1}{\epsilon} + \ln 4\pi - \gamma_{\rm E}, \tag{A3}$$

with $\gamma_{\rm E}$ being the Euler–Mascheroni constant.

Using the technique described in Ref. [74], the divergent parts are given by

$$\begin{aligned}&{\rm Div}[A_0(M_n)] = M_n^2\Delta_\epsilon, {\rm Div}[B_0^{(n)}] = {\rm Div}[B_0^{(12)}] = \Delta_\epsilon,\\ &{\rm Div}[B_1^{(1)}] = {\rm Div}[B_1^{(12)}] = \frac{1}{2}\Delta_\epsilon, {\rm Div}[B_1^{(2)}] = {\rm Div}[B_2^{(12)}] = -\frac{1}{2}\Delta_\epsilon.\end{aligned} \tag{A4}$$

Therefore, the above PV functions can be written in the form

$$\begin{aligned}&A_0(M) = M^2\Delta_\epsilon + a_0(M),\ B^{(n)}_{0,1} = {\rm Div}[B^{(n)}_{0,1}] + b^{(n)}_{0,1},\ B^{(12)}_{0,1,2}\\ &\quad = {\rm Div}[B^{(12)}_{0,1,2}] + b^{(12)}_{0,1,2},\end{aligned} \tag{A5}$$

where $a_0(M)$, $b^{(n)}_{0,1}$, and $b^{(12)}_{0,1,2}$ are finite parts and have specific forms, as defined in Refs. [17, 29, 75] for LFVHDs.

APPENDIX B. ANALYTIC FORMULAS AT ONE-LOOP ORDER TO $l_a \to l_a b\gamma$ AND $\mathrm{H} \to l_i l_j$.

In this section, we present the one-loop analytical expressions for the decays $l_a \to l_b\gamma$ and $\mathrm{H} \to l_i l_j$. Based on the couplings listed in Table 2, the decay $(l_a \to l_b\gamma)$ occurs only at the loop level. These contributions include $\mathcal{D}^{CH}_{L,R}(\nu_a, W^\pm)$, $\mathcal{D}^{CH}_{L,R}(\nu_a, V^\pm)$, $\mathcal{D}^{CH}_{L,R}(\nu_a, H^\pm_{1,2})$, and $\mathcal{D}^{CH}_{L,R}(N_a, H^\pm_1)$. They are given by [17, 22]:

$$\begin{aligned}\mathcal{D}^{CH}_{L,R}(\nu_a, W^\pm) &= -\frac{eg^2}{32\pi^2 m_W^2}\sum_{n=1}^{9} U^{\nu *}_{an} U^{\nu}_{bn} F(t_{nW}),\\ \mathcal{D}^{CH}_{L,R}(\nu_a, Y^\pm) &= -\frac{eg^2}{32\pi^2 m_Y^2}\sum_{n=1}^{9} U^{\nu *}_{(a+3)n} U^{\nu}_{(b+3)n} F(t_{nY}),\\ \mathcal{D}^{CH}_{L,R}(\nu_a, H^\pm_{1,2}) &= -\frac{eg^2 f_s}{16\pi^2 m_W^2}\sum_{k=1}^{9}\left[\frac{\lambda^{L,s*}_{ak}\lambda^{L,s}_{bk}}{m^2_{H^\pm_s}}\right.\\ &\quad\times\frac{1-6t_{ks}+3t_{ks}^2+2t_{ks}^3-6t_{ks}^2\ln(t_{ks})}{12(t_{ks}-1)^4}\\ &\quad\left.+\frac{m_{n_k}\lambda^{L,s*}_{ak}\lambda'^{R,s}_{bk}}{m^2_{H^\pm_s}}\frac{-1+t_{ks}^2-2t_{ks}\ln(t_{ks})}{2(t_{ks}-1)^3}\right],\\ \mathcal{D}^{CH}_{L,R}(N_a, H^\pm_1) &= -\frac{eg^2 f_s}{16\pi^2 m_W^2}\sum_{k=1}^{9}\left[\frac{\lambda^{L,s*}_{ak}\lambda^{L,s}_{bk}}{m^2_{H^\pm_s}}\right.\\ &\quad\left.+\frac{1-6t_{ks}+3t_{ks}^2+2t_{ks}^3-6t_{ks}^2\ln(t_{ks})}{12(t_{ks}-1)^4}\right],\end{aligned} \tag{B1}$$

where, we use symbols

$$t_{ks} = \left(\frac{m_{n_k}}{m_{H^\pm_s}}\right)^2,\ t_{nW} = \left(\frac{m_{n_n}}{m_{W^\pm}}\right)^2,\ t_{nY} = \left(\frac{m_{n_n}}{m_{Y^\pm}}\right)^2. \tag{B2}$$

The one-loop factors of the diagrams in Fig. 1 are given below. We use the same calculation techniques as those presented in [29], and the symmetry coefficients of the diagrams are taken from Refs. [76, 77]. We define $m_{l_i} \equiv m_1$ and $m_{l_j} \equiv m_2$.

$$\begin{aligned}\mathcal{M}^{(1)}_L(m_F, m_Y) = m_1\left\{\right.&\frac{1}{2m_Y^3}\left[m_F^2(B_1^{(1)} - B_0^{(1)} - B_0^{(2)})\right.\\ &\left.- m_2^2 B_1^{(2)} + \left(2m_V^2 + m_H^2\right)m_F^2(C_0 - C_1)\right]\\ &-\left(2m_Y + \frac{m_1^2 - m_2^2}{m_Y}\right)C_1\\ &\left.+\left(\frac{m_1^2 - m_H^2}{m_Y} + \frac{m_2^2 m_H^2}{2m_Y^3}\right)C_2\right\},\end{aligned} \tag{B3}$$

$$\begin{aligned}\mathcal{M}^{(1)}_R(m_F, m_Y) = m_2\left\{\right.&\frac{1}{2m_Y^3}\left[-m_F^2\left(B_1^{(2)} + B_0^{(1)} + B_0^{(2)}\right)\right.\\ &\left.+ m_1^2 B_1^{(1)} + (2m_V^2 + m_H^2)m_F^2(C_0 + C_2)\right]\\ &+\left(2m_Y - \frac{m_1^2 - m_2^2}{m_Y}\right)C_2\\ &\left.-\left(\frac{m_2^2 - m_H^2}{m_Y} + \frac{m_1^2 m_H^2}{m_Y^3}\right)C_1\right\},\end{aligned} \tag{B4}$$

$$\begin{aligned}&\mathcal{M}^{(2)}_L(a_1, a_2, v_1, v_2, m_F, m_Y, m_{H^\pm})\\ &= m_1\left\{-\frac{a_2}{v_2}\frac{m_F^2}{m_Y^2}\left(B_1^{(1)} - B_0^{(1)}\right) + \frac{a_1}{v_1}m_2^2\left[2C_1 - \left(1 + \frac{m_{H^\pm}^2 - m_H^2}{m_Y^2}\right)C_2\right]\right.\\ &\left.+\frac{a_2}{v_2}\frac{m_F^2}{m_Y^2}\left[(m_{H^\pm}^2 - m_H^2 + m_Y^2)C_0 + (m_H^2 - m_{H^\pm}^2 + m_Y^2)C_1\right]\right\},\end{aligned} \tag{B5}$$

$$\begin{aligned}&\mathcal{M}^{(2)}_R(a_1, a_2, v_1, v_2, m_F, m_Y, m_{H^\pm})\\ &= m_2\left\{\frac{a_1}{v_1}\left[\frac{m_1^2 B_1^{(1)} - m_F^2 B_0^{(1)}}{m_Y^2} + \left(m_F^2 C_0 - m_1^2 C_1 + 2m_2^2 C_2\right.\right.\right.\\ &\left.\left.\left.+2(m_H^2 - m_2^2)C_1 - \frac{m_{H^\pm}^2 - m_H^2}{m_Y^2}\left(m_F^2 C_0 - m_1^2 C_1\right)\right)\right]\right.\\ &\left.+\frac{a_2}{v_2}\frac{m_F^2}{m_Y^2}\left[-2m_Y^2 C_0 - (m_H^2 - m_{H^\pm}^2 + m_Y^2)C_2\right]\right\},\end{aligned} \tag{B6}$$

$$\mathcal{M}_L^{(3)}(a_1,a_2,v_1,v_2,m_F,m_{H^\pm},m_Y) = m_1\left\{\frac{a_1}{v_1}\left[-\frac{m_2^2B_1^{(2)}+m_F^2B_0^{(2)}}{m_Y^2}+\Big(\, m_F^2C_0-2m_1^2C_1+m_2^2C_2 \right.\right.$$
$$\left.\left.+2(m_1^2-m_H^2)C_2+\frac{m_H^2-m_{H^\pm}^2}{m_Y^2}\left(m_F^2C_0+m_2^2C_2\right)\Big)\right]+\frac{a_2}{v_2}m_F^2\left(-2C_0+\frac{m_Y^2+m_{H^\pm}^2-m_H^2}{m_Y^2}C_1\right)\right\}, \tag{B7}$$

$$\mathcal{M}_R^{(3)}(a_1,a_2,v_1,v_2,m_F,m_{H^\pm},m_Y) = m_2\left\{\frac{a_2}{v_2}\frac{m_F^2}{m_Y^2}\left(B_1^{(2)}+B_0^{(2)}\right)+\frac{a_1}{v_1}m_1^2\left[-2C_2+\left(1+\frac{m_{H^\pm}^2-m_H^2}{m_Y^2}\right)C_1\right]\right.$$
$$\left.+\frac{a_2}{v_2}\frac{m_F^2}{m_Y^2}\left[(m_Y^2+m_{H^\pm}^2-m_H^2)C_0+(m_{H^\pm}^2-m_H^2-m_Y^2)C_2\right]\right\}. \tag{B8}$$

$$\mathcal{M}_L^{(4+5)}(m_F,m_Y) = \frac{-m_1m_2^2}{m_Y^3(m_1^2-m_2^2)}\left[\left(2m_Y^2+m_F^2\right)\left(B_1^{(1)}+B_1^{(2)}\right)+m_1^2B_1^{(1)}+m_2^2B^{(2)}-2m_F^2\left(B_0^{(1)}-B_0^{(2)}\right)\right], \tag{B9}$$

$$\mathcal{M}_R^{(4+5)}(m_F,m_Y) = \frac{m_1}{m_2}\mathcal{M}_L^{(4+5)}(m_F,m_Y), \tag{B10}$$

$$\mathcal{M}_L^{(6)}(a_1,a_2,v_1,v_2,m_F,m_{H^\pm}) = \frac{m_1m_F^2}{v_2}\times\left[\frac{a_1^2}{v_1^2}m_2^2(2C_2+C_0)+\frac{a_2^2}{v_2^2}m_F^2(C_0-2C_1)\right.$$
$$\left.+\frac{a_1a_2}{v_1v_2}\left(B_0^{(12)}+(m_F^2+m_{H^\pm}^2+m_2^2)C_0+2m_2^2C_2-(m_1^2+m_2^2)C_1\right)\right], \tag{B11}$$

$$\mathcal{M}_R^{(6)}(a_1,a_2,v_1,v_2,m_F,m_{H^\pm}) = \frac{m_2m_F^2}{v_2}\times\left[\frac{a_1^2}{v_1^2}m_1^2(C_0-2C_1)+\frac{a_2^2}{v_2^2}m_F^2(C_0+2C_2)\right.$$
$$\left.+\frac{a_1a_2}{v_1v_2}\left(B_0^{(12)}+(m_F^2+m_{H^\pm}^2+m_1^2)C_0-2m_1^2C_1+(m_1^2+m_2^2)C_2\right)\right], \tag{B12}$$

$$\mathcal{M}_L^{(7)}(a_1,a_2,v_1,v_2,m_F,m_{H^\pm}) = m_1v_2\left[\frac{a_1a_2}{v_1v_2}m_F^2C_0+\frac{a_2^2}{v_2^2}m_F^2C_1-\frac{a_1^2}{v_1^2}m_2^2C_2\right], \tag{B13}$$

$$\mathcal{M}_R^{(7)}(a_1,a_2,v_1,v_2,m_F,m_{H^\pm}) = m_2v_2\left[\frac{a_1a_2}{v_1v_2}m_F^2C_0+\frac{a_1^2}{v_1^2}m_1^2C_1-\frac{a_2^2}{v_2^2}m_F^2C_2\right], \tag{B14}$$

$$\mathcal{M}_L^{(8)}(m_Y,m_F) = \frac{m_1m_F^2}{m_Y^3}\times\left[\left(B_0^{(12)}+B_1^{(1)}-(m_1^2+m_2^2-2m_F^2)C_1\right)-(C_0-4C_1)m_Y^2\right], \tag{B15}$$

$$\mathcal{M}_R^{(8)}(m_Y,m_F) = \frac{m_2m_F^2}{m_Y^3}\times\left[\left(B_0^{(12)}-B_1^{(2)}+(m_1^2+m_2^2-2m_F^2)C_2\right)-(C_0+4C_2)m_Y^2\right], \tag{B16}$$

$$\mathcal{M}_L^{(9+10)}(a_1,a_2,v_1,v_2,m_F,m_{H^\pm}) = \frac{m_1}{(m_1^2-m_2^2)v_1}\left[m_2^2\left(m_1^2\frac{a_1^2}{v_1^2}+m_F^2\frac{a_2^2}{v_2^2}\right)\left(B_1^{(1)}+B_1^{(2)}\right)+m_F^2\frac{a_1a_2}{v_1v_2}\left(2m_2^2B_0^{(1)}-(m_1^2+m_2^2)B_0^{(2)}\right)\right], \tag{B17}$$

$$\mathcal{M}_R^{(9+10)}(a_1,a_2,v_1,v_2,m_F,m_{H^\pm}) = \frac{m_2}{(m_1^2-m_2^2)v_1}\left[m_1^2\left(m_2^2\frac{a_1^2}{v_1^2}+m_F^2\frac{a_2^2}{v_2^2}\right)\left(B_1^{(1)}+B_1^{(2)}\right)+m_F^2\frac{a_1a_2}{v_1v_2}\left(-2m_1^2B_0^{(2)}+(m_1^2+m_2^2)B_0^{(1)}\right)\right]. \tag{B18}$$

In the seventh diagram of Fig. 1, we find that $\mathcal{M}^{(7)}_{L,R}(a_1,a_2,v_1,v_2,m_F,m_H)$ is always finite because C_k $(k=0,1,2)$ does not contain divergent functions.

References

[1] Z. Calcuttawala, A. Kundu, S. Nandi *et al.*, Phys. Rev. D **97**(9), 095009 (2018)
[2] X. S. Yan, Z. Q. Hu, Q. Chang *et al.*, Phys. Rev. D **112**(5), 055026 (2025)
[3] L. Oleg, B. Sergei, and V. Mikhail, Eur. Phys. J. C **67**(7), 213 (2010)
[4] C. Patrignani *et al.* (Particle Data Group), Chin. Phys. C **40**(10), 100001 (2016)
[5] M. Tanabashi *et al.* (Particle Data Group), Phys. Rev. D **98**(3), 030001 (2018)
[6] S. Navas *et al.* (Particle Data Group), Phys. Rev. D **110**(3), 030001 (2024)
[7] G. Aad *et al.* (ATLAS Collaboration), Phys. Lett. B **796**, 68 (2019)
[8] P. A. Zyla *et al.* (Particle Data Group), PTEP **2020**(8), 083C01 (2020)
[9] B. Aubert *et al.* (BaBar Collaboration), Phys. Rev. Lett. **104**, 021802 (2010)
[10] A. M. Baldini *et al.* (MEG Collaboration), Eur. Phys. J. C **76**, 434 (2016)
[11] A. M. Sirunyan *et al.* (CMS Collaboration), JHEP. **06**, 120 (2018)
[12] G. Aad *et al.* (ATLAS Collaboration), Phys. Lett. B **800**, 135069 (2020)
[13] G. Aad *et al.* (ATLAS Collaboration), Phys. Lett. B. **801**, 135148 (2020)
[14] J. K. Mizukoshi, C. A. de S.Pires, F. S. Queiroz *et al.*, Phys. Rev. D **83**, 065024 (2011)
[15] A. G. Dias, C. A. de S.Pires, and P. S. R. da Silva, Phys. Lett. B **628**, 85 (2005)
[16] H. T. Hung and A. B. Arbuzov, Chin.Jour. Phys **102**, 264 (2026)
[17] H. T. Hung, D. T. Binh, and H. V. Quyet, Chin. Phys. C. **46**(12), 123104 (2022)
[18] J. C. Montero, F. Pisano, and V. Pleitez, Phys. Rev. D **47**(7), 2918 (1993)
[19] S. M. Boucenna, J. W. F. Valle, and V. Avelino, Phys. Rev. D **92**, 053001 (2015)
[20] C. Hernandez, A. Enrique, R. Martinez *et al.*, Eur. Phys. J. C **C76**, 634 (2016)
[21] T. P. Nguyen, T. T. Le, T. T. Hong *et al.*, Phys. Rev. **D97**, 073003 (2018)
[22] H. T. Hung, N. T. Tham, T. T. Hieu *et al.*, PTEP. **2021**(8), 083B01 (2021)
[23] M. M. Ferreira, T. B. de Melo, S. Kovalenko *et al.*, Eur. Phys. J. C **79**(11), 955 (2019)
[24] A. E. C. Hernandez, J. M. Gonzalez, and U. J. Saldana-Salazar, Phys. Rev. D **100**, 035024 (2019)
[25] M. E. Catano, R. Martinez, and F. Ochoa, Phys. Rev. D **86**, 073015 (2012)
[26] A. E. C. Hernandez, M. E. Catano, and R. Martinez, Phys. Rev. D **90**, 073001 (2014)
[27] A.G. Dias, C. A. de S.Pires, P. S. R. da Silva *et al.*, Phys. Rev. D **86**, 035007 (2012)
[28] L.T. Hue, H. N. Long, T. T. Thuc *et al.*, Nucl. Phys. B **907**, 37 (2016)
[29] T. T. Thuc, L.T. Hue, H. N. Long *et al.*, Phys. Rev. D **93**, 115026 (2016)
[30] H. B. Zhang, T. F. Feng, S. M. Zhao *et al.*, Chin. Phys. C **41**, 043106 (2017)
[31] J. Herrero-Garcia, T. Ohlsson, S. Riad *et al.*, JHEP **04**, 130 (2017)
[32] G. Blankenburg, J. Ellis, and G. Isidori, Phys. Lett. B **712**, 386 (2012)
[33] A. Pilaftsis, Phys. Lett. B **285**, 68 (1992)
[34] J. Herrero-Garcia, N. Rius, and A. Santamaria, JHEP **11**, 084 (2016)
[35] T. T. Hong, L. T. T. Phuong, T. P. Nguyen *et al.*, Phys. Rev. D **110**(7), 075010 (2024)
[36] T. T. Hong, L. T.Hue, L. T. T. Phuong *et al.*, Phys. Scripta **99**(12), 125308 (2024)
[37] N. T. Duy, D. T. Huong, D. van Loi *et al.*, Eur. Phys. J. C **85**(9), 1053 (2025)
[38] A. M. Sirunyan *et al.* (CMS Collaboration), JHEP **03**, 103 (2020)
[39] A. M. Sirunyan *et al.* (CMS Collaboration), JHEP **07**, 208 (2021)
[40] A. G. Dias, C. A. de S. Pires, and P. S. Rodrigues da Silva, Phys. Rev. D **68**, 115009 (2003)
[41] A. G. Dias and V. Pleitez, Phys. Rev. D **69**, 077702 (2004)
[42] A. G. Dias and V. Pleitez,. and M. D. Tonasse, Phys. Rev. D **67**, 095008 (2003)
[43] J. G. Ferreira, C. A. de S. Pires, J. G. Rodrigues *et al.*, Phys. Lett. B **771**, 199 (2017)
[44] V. H. Binh, D. T. Binh, A. E. C. Hernández *et al.*, Phys. Rev. D **107**, 095030 (2023)
[45] D. Chang and H. N. Long, Phys. Rev. D **73**, 053006 (2006)
[46] H. N. Long, H. T. Hung, V. H. Binh *et al.*, (2024), arXiv: 2412.04269 [hep-ph]
[47] A. Ibarra, E. Molinaro, and S. T. Petcov, JHEP **09**, 108 (2010)
[48] H. N. Long and T. Inami, Phys. Rev. D **61**, 075002 (2000)
[49] A. G. Dias, V. Pleitez, and M. D. Tonasse, Phys. Rev. D **69**, 015007 (2004)
[50] A. Crivellin, M. Hoferichter, and P. Schmidt-Wellenburg, Phys. Rev. D. **98**, 113002 (2018)
[51] H. V. Quyet, T. T. Hieu, N. T. Tham *et al.*, Chin. J. Phys. **90**, 166 (2024)
[52] H. T. Hung, T. T. Hong, H. H. Phuong *et al.*, Phys. Rev. D **100**, 075014 (2019)
[53] A. Denner, S. Heinemeyer, I. Puljak *et al.*, Eur. Phys. J. C **71**, 1753 (2011)
[54] S. Chatrchyan *et al.* (CMS Collaboration), Phys. Lett. B **710**, 403 (2012)
[55] S. Chatrchyan *et al.* (CMS Collaboration), Phys. Lett. B **710**, 26 (2012)
[56] V. Barger, M. Ishida, and W. Y. Keung, Phys. Rev. Lett. **108**, 261801 (2012)
[57] A. Abusleme *et al.* (JUNO Collaboration), Prog. Part. Nucl. Phys. **123**, 103927 (2022)
[58] L. T. Hue, K. H. Phan, T. P. Nguyen *et al.*, Eur. Phys. J. C. **82**(8), 722 (2022)

[59] J. R. Andersen *et al*., CERN-2013-004, month 7, (2013), arXiv: 1307.1347[hep-ph]
[60] U. Langenfeld, S. O. Moch, and T. Pfoh, JHEP **11**, 070 (2012)
[61] G. Das and S. O. Moch, TTK-25-34, P3H-25-080, 10.21468/SciPostPhysCommRep.17, (2025)., arXiv: 2510.17413[hep-ph]
[62] C. Anastasiou, C. Duhr, F. Dulat *et al*., JHEP **05**, 058 (2016)
[63] J. Davies, F. Herren, and M. Steinhauser, Phys. Rev. Lett. **124**(11), 112002 (2020)
[64] R. V. Harlander *et al*., Eur.Phys.J C **66**, 359 (2010)
[65] Le Duc Ninh and H. N. Long, Phys. Rev. D **72**, 075004 (2005)
[66] M. A. Perez, G. Tavares-Velasco, and J. J. Toscano, Phys. Rev. D **69**, 115004 (2004)
[67] P. Athron, D. Harries, and A. G. Williams, Phys. Rev. D **91**, 115024 (2015)
[68] M. Cvetic and P. Langacker, Adv. Ser. Direct. High Energy Phys. **18**, 312 (1998)
[69] M. Cannoni, Eur. Phys. J. C **76**(3), 137 (2016)
[70] G. Bertone, D. Hooper, and J. Silk, Phys. Rept. **405**, 279 (2005)
[71] N. Aghanim *et al*., Astron. Astrophys. **641**, A6 (2020)
[72] N. A. Bahcall, J. P. Ostriker, S. Perlmutter *et al*., Science **248**, 1481 (1999)
[73] G. Passarino and M. J. G. Veltman, Nucl. Phys. B **160**, 151 (1979)
[74] L. T. Hue, L. D. Ninh, T. T. Thuc *et al*., Eur. Phys. J. C **78**(2), 128 (2018)
[75] K. H. Phan, H. T. Hung, and L.T. Hue, PTEP **2016**(11), 113B03 (2016)
[76] L. T. Hue, H. T. Hung, and H. N. Long, Rept. Math. Phys. **69**, 331 (2012)
[77] P. V. Dong, L. T. Hue, H. T. Hung *et al*., Theor. Math. Phys. **165**, 1500 (2010)